frontiers in Earth Science

ORIGINAL RESEARCH
published: 25 October 2021
doi: 10.3389/feart.2021.729905

Geochronology and Petrogenesis of Early Pleistocene Dikes in the Changbai Mountain Volcanic Field (NE China) Based on Geochemistry and Sr-Nd-Pb-Hf Isotopic Compositions

Meng-Meng Li[1,2,3], *Zhi-Tao Xu*[1,2,3]*, *Guido Ventura*[4,5], *Xiao-Dong Pan*[1,2], *Di Han*[1,2], *Guo-Hui Gu*[1,2], *Dong-Han Yan*[1,2], *Bo Pan*[6] and *Jing-Qiao Feng*[3]

[1]Institute of Volcanology, China Earthquake Administration, Changchun, China, [2]Jilin Earthquake Agency, Changchun, China, [3]Jilin Engineering Earthquake Research Center, Changchun, China, [4]Istituto Nazionale di Geofisica e Vulcanologia, Rome, Italy, [5]Istituto per lo Studio degli Impatti Antropici e Sostenibilità in Ambiente Marino, Consiglio Nazionale delle Ricerche (CNR), Capo Granitola (TP), Campobello di Mazara, Italy, [6]Jilin Changbaishan Volcano National Observation and Research Station, Institute of Geology, China Earthquake Administration, Beijing, China

OPEN ACCESS

Edited by:
Paterno Castillo,
University of California, San Diego,
United States

Reviewed by:
Kwan-Nang Pang,
Institute of Earth Sciences, Taiwan
Yang Sun,
Southern University of Science and Technology, China

***Correspondence:**
Zhi-Tao Xu
xuzhjtao@163.com

Specialty section:
This article was submitted to Petrology, a section of the journal Frontiers in Earth Science

Received: 29 June 2021
Accepted: 16 September 2021
Published: 25 October 2021

Citation:
Li M-M, Xu Z-T, Ventura G, Pan X-D, Han D, Gu G-H, Yan D-H, Pan B and Feng J-Q (2021) Geochronology and Petrogenesis of Early Pleistocene Dikes in the Changbai Mountain Volcanic Field (NE China) Based on Geochemistry and Sr-Nd-Pb-Hf Isotopic Compositions. Front. Earth Sci. 9:729905. doi: 10.3389/feart.2021.729905

Changbai Mountains intraplate volcanism (NE China) developed above the 500 km deep stagnant portion of the Pacific slab in the last 20 Ma. The more recent activity includes a shield-forming stage (2.8–0.3 Ma), the Tianchi cone construction stage (1.5–0.01 Ma), and a caldera-forming stage (0.2 Ma-present). Detailed studies on the petrogenesis of the volcanic products between the first two stages and the possible role of geodynamics and local tectonics in controlling the volcanism, however, are lacking. Here, we present structural and whole-rock geochemical and zircon Hf isotopic data on Pleistocene dikes of the Changbai Mountains at the transition from the shield-forming to the Tianchi stage with the aim to constrain their age and the source(s) of their parental magma. The dikes represent the shallower feeding system of monogenetic cones and have a NW-SE strike, which is also the preferred strike of the major fault affecting the area and along which the Changbai Mountains monogenetic scoria cones align. The dikes have a potassic affinity and a trachybasaltic composition. Their zircon U–Pb age is 1.19–1.20 Ma (Calabrian). The trachybasalts are enriched in Rb, Ba, Th, U, Nb, Ta, K, Pb, and LREE and slightly depleted in Sr, Zr, Hf, Ti, and HREE with a weak negative Eu/Eu* (δEu = 0.96–0.97). Trace elements and isotopic compositions are compatible with an OIB-type source with an EMI signature. The calculated $(^{87}Sr/^{86}Sr)_i$ (=0.705165–0.705324), $(^{143}Nd/^{144}Nd)_i$ (= 0.512552–0.512607, εNd(t) = −0.58 to −1.65), and Hf model ages (T_{DM2}) of 1768–1562 Ma suggest that the trachybasaltic dikes were contaminated by a Mesoproterozoic, relatively basic lower crust. The source of the Calabrian trachybasalts consists of asthenospheric melts modified by a subcontinental lithospheric mantle. These melts upwell from depth and stop at the crust-mantle interface where underplating processes favor the assimilation of ancient lower crust material. During the ascent to the surface along deep-seated crustal discontinuities, these magmas weakly differentiate.

Keywords: dikes, intraplate magmatism, OIB-EM1 sources, zircon U–Pb dating, Sr-Nd-Pb-Hf isotopes, Changbai Mountains-Tianchi 3

HIGHLIGHTS

1) Trachybasalt dikes in Changbaishan volcanic area are controlled by a major crustal discontinuity.
2) The trachybasalt dikes were formed at the Calabrian stage of the early Pleistocene (1.19–1.20 Ma).
3) An OIB source with EM1 signature assimilates Mesoproterozoic crust by underplating processes.
4) Intraplate volcanism above stagnant slabs involves three sources: asthenosphere, slab-derived fluids, and ancient crustal rocks.

INTRODUCTION

The eastern China block includes the eastern margin of the Central Asian orogenic belt (the Xing'an-Mongolia orogenic belt), the North China Craton (NCC), the Sulu-Dabie high pressure orogeny belt, the Yangtze Craton, and the southeast coastal orogenic belt of China, and it is characterized by Mesozoic volcanic and intrusive rocks (**Figure 1A**). The later Cenozoic volcanic rocks mainly consist of basalts emitted in an intraplate setting (e.g., Wu et al., 2011; Zhang and Luo, 2011; Deng et al., 2017) associated to metallogenic and hydrothermal deposits (Sun et al., 2012, 2013; Deng et al., 2017). Changbai Mountains, which consist of basaltic shields, monogenetic vents, and central-type volcanoes, are located above the 500 km deep stagnant slab of the westward subducting Pacific plate (**Figure 1A**). Three main geodynamic models have been suggested to explain the Changbai Mountain volcanism: an upwelling mantle plume (Mao et al., 1999), an intraplate continental rifting (Gilder et al., 1991), and the Pacific plate subduction (e.g., Mao et al., 2013; Ouyang et al., 2014; Zhang et al., 2014; Xu W. L. et al., 2020; Xu Z.-t. et al., 2020). Previous studies on the Changbai Mountains area mainly focus on the Holocene silicic magmatism (e.g., Wei et al., 2007; Liu et al., 2009; Xu J. D. et al., 2013a). The widely distributed early Pleistocene rocks are less known. The origin of the Pleistocene magmatism is still debated and different hypotheses have been proposed: 1) low degrees of partial melting of the asthenospheric mantle (Xu, et al., 2020a) possibly contaminated by the addition of crustal material (Sun et al., 2015); 2) partial melting of the subducted slab (Ma et al., 2015); 3) involvement of DM and EM1 end-members (Basu et al., 1991) or OIB and EM1 end-members (Xu et al., 2012); 4) an asthenospheric source metasomatized by recycled subducted silicate sediments or a subcontinental lithospheric mantle (EM1-like) and by carbonated eclogites with a MORB signature (Choi et al., 2020); and 5) an EM1-like source originated from the contamination of an OIB asthenospheric mantle by Paleoproterozoic lithosphere (Lee et al., 2021). Therefore, questions regarding the nature of the mantle and possible crustal sources of the Changbaishan Mountain volcanism and of the dynamics of the Pacific plate subduction remain open. In this study, we carried out systematic LA-MC-ICP-MS zircon U–Pb geochronology as well as whole-rock geochemistry, Sr-Nd-Pb isotopic analyses, and zircon Hf isotopic analyses to investigate the petrogenesis of the dikes related to the early Pleistocene monogenetic activity in area. The results allow us to improve our understanding of the petrogenesis and tectonic setting of the Changbai Mountains magmatism. New data and constraints on the relative role of the asthenosphere, ancient crust, and stagnant slab in the evolution of intraplate volcanism are provided.

GEOLOGICAL SETTING

The NE China magmatism mainly developed during Mesozoic and Cenozoic (Ge et al., 2003; Wu et al., 2005; Sun et al., 2007) eras. Because of continental rifting processes (Gilder et al., 1996; Zhou and Li, 2000; Zhu et al., 2011), the Changbai Mountain volcanic field (CMVF) is bounded by two NE-NW striking regional fault systems, the Dunhua-Mishan faults to the northeast and the Xar Morron-Changchun faults to the southeast although faults with a NW-SE strike are also locally present (**Figure 1B**). The origin of the latter faults is unclear, and they may represent the response of the NE China terrains to different rates of rifting associated to the Pacific slab roll-back. The basement of CVMF consists of Precambrian metamorphic rocks including Archean tonalite, trondhjemite, granodiorite (2.4–2.5 Ga) and Proterozoic quartzite, schists, and granulite assemblages (1.7–1.9 Ga) (Jin and Zhang, 1994; Wang et al., 2003). The CMVF volcanic rocks were emitted by three stratovolcanoes located at the China/North Korea boundary: the Tianchi caldera (last eruption in 1903) and the now inactive Wangtian'e in China and Namphothe edifices in North Korea. Several monogenetic scoria cones surround these three large stratovolcanoes. They roughly align along a NW-SE direction (inset in **Figure 1**). This direction is the same of the main fault affecting the Tianchi caldera (Baishan-Jince fault in **Figure 1**). After a basaltic plateau forming phase developed between 20 and 3 Ma, the volcanism in the Tianchi area can be roughly divided in three stages: 1) shield-forming stage (2.8–0.3 Ma), 2) the Tianchi cone construction stage (1.5–0.01 Ma), and 3) caldera-forming, explosive eruption stage (0.2 Ma-present) (Fan et al., 1999; Liu et al., 2015; Takeshi et al., 2020). Monogenetic volcanism mainly developed during the shield-forming stage, although some vents formed also during the cone construction stage. The early two stages were characterized by the emission of basaltic lava flows and scorias, while trachytes and rhyolites were emitted as lava flows and pyroclastic fall and flows, and these intermediate-acid magmatism mainly occurred in the last stage of basaltic magmatism.

The study area is located in the northern sector of the Tianchi area (**Figure 1B**). Here, the basement rocks include gneiss of the Paleoarchean Sidaolazi formation, amphibolite of the Yangjiadian formation, and quartz schist of the Mesoproterozoic Huashan formation. The volcanic rocks consist of Pleistocene and Pliocene basaltic lava flows and minor scorias (**Figure 2**). The products studied here are two dikes representing the shallowest feeding system of two neighbors, partly dismantled cones constituted by oxidized scorias and ash (**Figure 2**). Dike 1 strikes NNW-

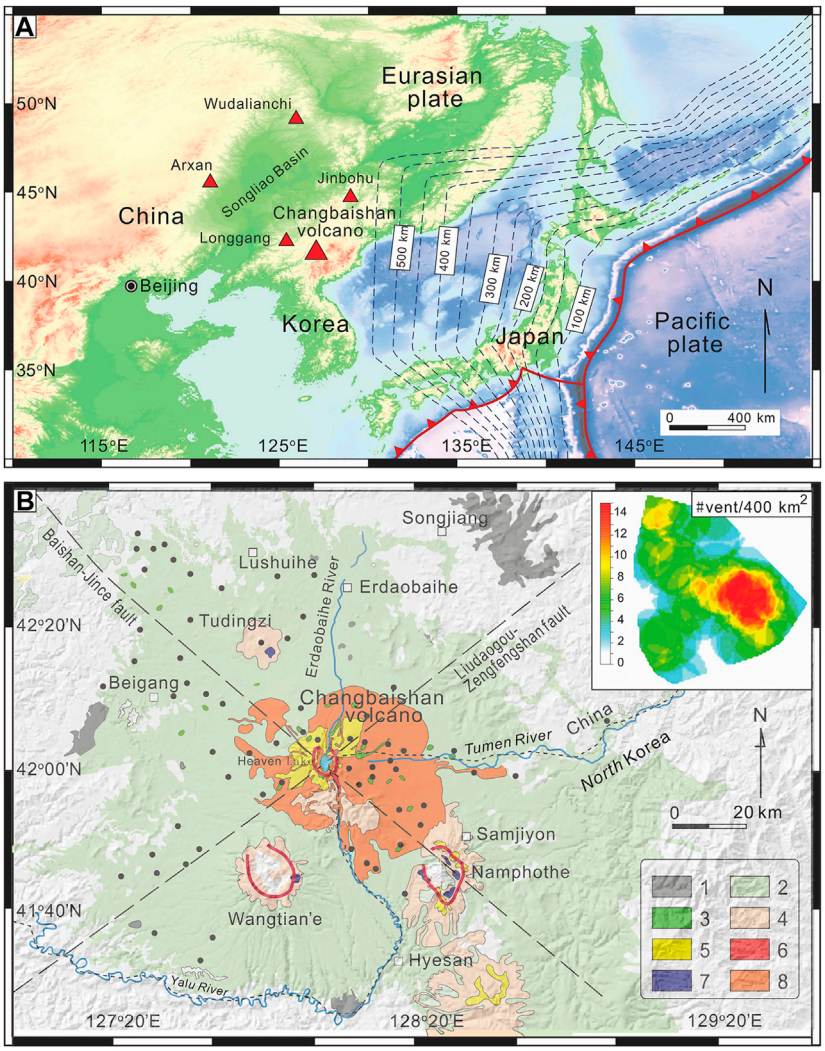

FIGURE 1 | (A) Schematic map showing location of the Changbaishan and other major volcanoes in NE China. The Japan trench is reported as red solid line with triangles and the depth of the Pacific slab is reported as dashed lines; the number indicates the depth in km (modified from Zhang et al., 2018; Chen et al., 2021; Fan et al., 2021; Sun et al., 2021). **(B)** Geological map of the Changbai Mountains volcanic field showing distribution of polygenetic (Changbaishan (Tianchi), Wangtian'e, and Namphothe and monogenetic (gray dots) volcanoes. Geological map legend: 1, pre-shield basalts; 2, shield-forming basalts; 3, post-shield basalts; 4, intermediate to silicic volcanic rocks (mainly trachyte with minor trachyandesite); 5, intermediate to silicic volcanic rocks (mainly trachyte with minor trachyandesite); 6, early rhyolite; 7, rhyolite; 8, pyroclastic deposits (primarily trachytic and rhyolitic in composition) erupted by caldera-forming eruptions of Tianchi. The inset on the top right reports the spatial density of monogenetic vents.

SSE; it is15–20 m long and 0.4–1.8 m thick. Dike 2 strikes NW-SE with dip 80°–85°; it is about 30 m long and 0.7–5.2 m thick with some lateral digitations having length of less than 2 m (**Figures 3A,B**). These dikes have 5–15 mm wide vesicles testifying the degassing of magma near the surface (**Figures 3C,D**).

SAMPLING AND ANALYTICAL TECHNIQUES

The sampling locations are shown in **Figure 2**. Unaltered, fresh samples were selected for a combined study involving whole-rock major and trace elements analyses, cathodoluminescence (CL) imaging, zircon U–Pb ages, and whole-rock Sr-Nd-Pb isotopes and zircon Hf isotopic analyses.

Sample Descriptions

The dikes are dark gray in color, massive to poorly vesiculated, and show a trachytic texture with plagioclases phenocrysts representing 80–85 vol% of the total minerals (**Figures 3E,F**). Clinopyroxene and biotite account for 5–10 vol% of the phenocrysts. The groundmass includes fine-grained plagioclase, pyroxene, amphibole, zircon (**Figures 3G,H**), apatite, and magnetite microlites. No significant differences in mineral assemblage, texture, and crystal content have been recognized between the two dikes.

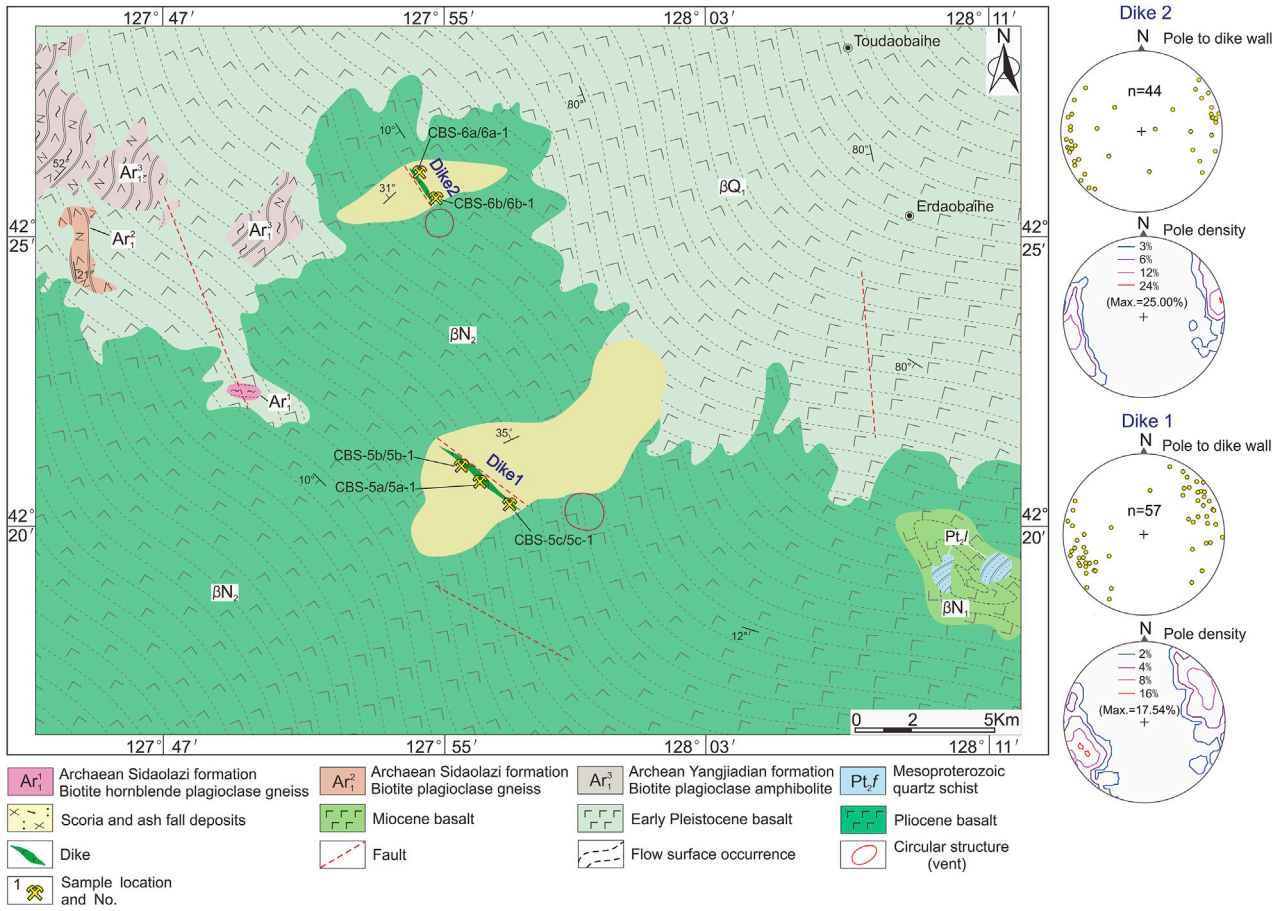

FIGURE 2 | Geological sketch map of the study region (after BGMRJP, 1988) with the location of the monogenetic vents and of the collected samples. On the right, the measured poles to the dike walls in Dike 1 and Dike 2 are shown. Density contours of the poles are also reported.

LA-MC-ICP-MS Zircon U–Pb Dating

Zircon was mounted in epoxy discs, polished to expose the grains, cleaned ultrasonically in ultrapure water, and then cleaned again prior to the analysis using AR grade methanol. Pre-ablation was conducted for each spot analysis using 5 laser shots (~0.3 μm in depth) to remove potential surface contamination. The analysis was performed using 30 μm diameter spot at 5 Hz and a fluence of 2 J/cm^2. Zircon U–Pb dating was conducted using LA-MC-ICP-MS (laser ablation multiple collector inductively coupled plasma mass spectrometry) in Nanjing Hong Chuang Geological Exploration Technology Service Company Limited (NHGETSCL). The Resolution SE model laser ablation system (Applied Spectra, United States) was equipped with ATLEX 300 excimer laser and a two volume S155 ablation cell. The laser ablation system was coupled to a Neptune Plus MC-ICP-MS (Wrexham, Wales, United Kingdom). Detailed tuning parameters can be seen in Thompson et al. (2018). Iolite software package was used for data reduction (Paton et al., 2010). Zircon 91500 and GJ-1 were used as primary and secondary reference materials, respectively. 91500 was analyzed twice and GJ-1 analyzed once every 10–12 analyses of the sample. The age of GJ-1 (604 ± 6 Ma, 1 σ) measured during the experiment was consistent with the recommended values within the uncertainty range, and the preferred value of 91500 is in Wiedenbeck et al. (1995); the ^{207}Pb/^{206}Pb and ^{206}Pb/^{238}U age of 91500 is 1065.4 and 1062.4 Ma. Based on the decay coefficient, Th/U ratio, and the error of the measurements in young zircons, we corrected the age loss caused by ^{203}Th depletion (Zou et al., 2010). The LA-MC-ICP-MS U–Pb isotopic data are listed in **Table 1**.

Zircon Lu–Hf Isotopic Analyses

Experiments of *in situ* Hf isotope ratio analysis were conducted using the Teledyne Cetac Technologies Analyte Excite laser ablation system (Bozeman, Montana, United States) and the Nu Instruments Nu Plasma II MC-ICP-MS (Wrexham, Wales, United Kingdom) that were hosted at the State Key Laboratory for Mineral Deposits Research, Nanjing University. The 193 nm ArF excimer laser, homogenized by a set of beam delivery systems, was focused on zircon surface with fluence of 6.0 J/cm^2. Ablation protocol employed a spot diameter of 50 um at 8 Hz repetition rate for 40 s. Helium

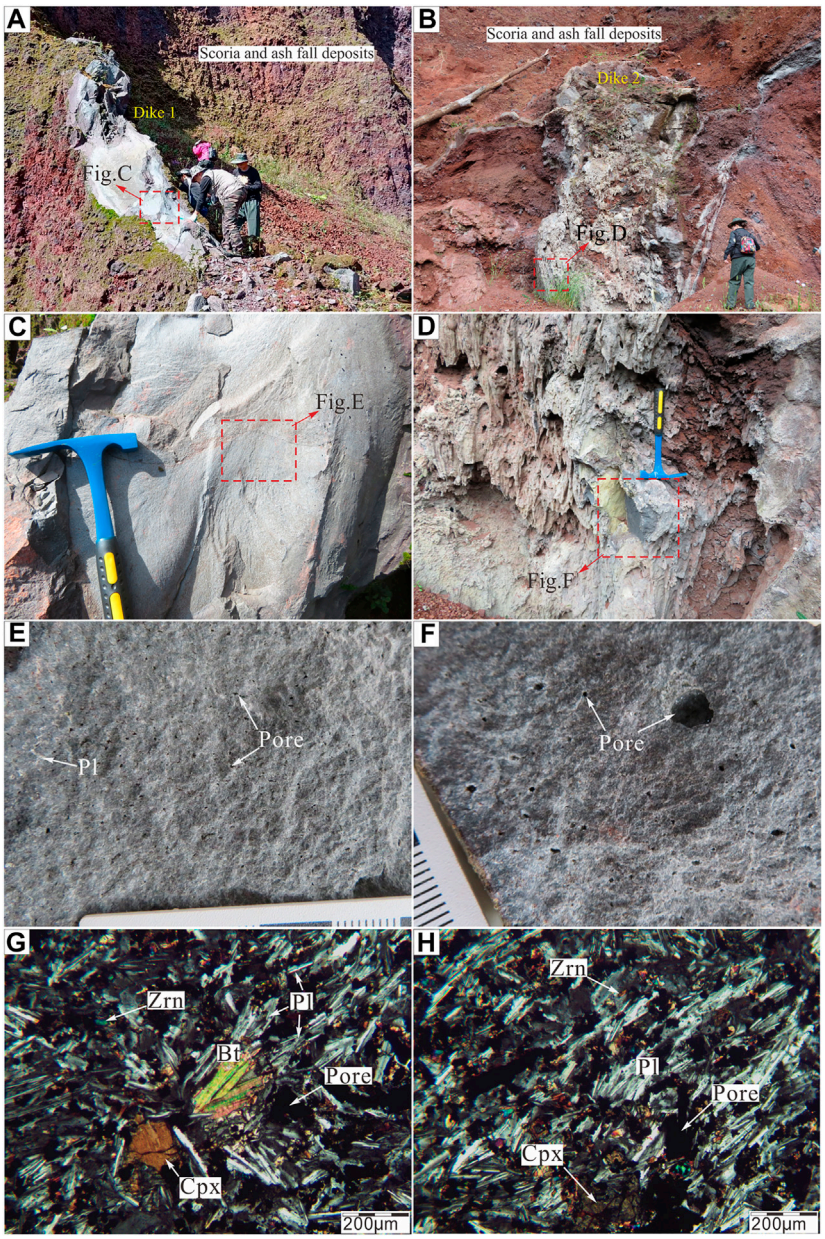

FIGURE 3 | Field photographs **(A–D)**, typical hand specimens **(E, F),** and photomicrographs **(G, H)** of the trachybasalt dikes in the study area. Abbreviations: Bt = biotite; Cpx = clinopyroxene; Pl = plagioclase; Zrn = zircon.

was applied as carrier gas to efficiently transport aerosol to MC-ICP-MS; the results of the zircon Hf isotopic analyses are given in **Table 2**. The precision of sample test is 0.000005–0.000012 (0.015–0.04‰, 2 s), and the accuracy is better than 0.000 012 (~0.04‰).

Major and Trace Element Determinations

The geochemical sample analyses were performed at the State Key Laboratory of Lithospheric Evolution, Institute of Geology and Geophysics, Chinese Academy of Sciences. The major element oxides were analyzed by a Panalytical PW4400 X-ray fluorescence spectrometer (AxiosmAX, Holland). The detailed sample-digesting procedure was as follows: 1) sample powder (200 mesh) were placed in an oven at 105°C for drying of 12 h. 2) ~1.0g dried sample was accurately weighted and placed in the ceramic crucible and then heated in a muffle furnace at 1000°C for 2 h. After cooling to 400°C, this sample was placed in the drying vessel and weighted again in order to calculate the loss on ignition (LOI). 3) 0.6 g sample powder was mixed with 6.0 g cosolvent and 0.3 g oxidant in a Pt crucible, which was placed in the furnace at 1150°C for 14 min. Then, the sample was

TABLE 1 | LA-MC-ICP-MS zircon U–Pb data of trachybasalt dike from the Changbai Mountain volcanic rock area.

Sample No.	Th	U	Th/U	Isotope ratio										Age/Ma							
	ppm			$^{207}Pb/^{235}U$	1σ	$^{206}Pb/^{238}U$	1σ	$^{238}U/^{206}Pb$	1σ	$^{207}Pb/^{206}Pb$	1σ	$^{208}Pb/^{232}Th$	1σ	$^{207}Pb/^{235}U$	1σ	$^{206}Pb/^{238}U$	1σ	$^{207}Pb/^{206}Pb$	1σ	$^{208}Pb/^{232}Th$	1σ
Trachybasalt dike 1, CBS-5a, mean = 1.19 ± 0.0057 Ma, *n* = 15																					
CBS-5a-1	5893	2373	2.5	0.001271	0.000029	0.0001874	0.0000010	5336.179	28.47481	0.04900	0.0011	0.0000629	0.0000004	1.29	0.03	1.21	0.01	137.00	50.00	1.27	0.01
CBS-5a-2	2046	1336	1.5	0.001382	0.000035	0.0001870	0.0000010	5347.594	28.59676	0.05360	0.0014	0.0000641	0.0000005	1.40	0.04	1.21	0.01	309.00	55.00	1.30	0.01
CBS-5a-3	4131	2138	1.9	0.001247	0.000028	0.0001862	0.0000010	5371.723	27.98975	0.04880	0.0011	0.0000626	0.0000004	1.27	0.03	1.20	0.01	120.00	48.00	1.27	0.01
CBS-5a-4	3684	1842	2.0	0.001326	0.000039	0.0001836	0.0000013	5446.623	38.56541	0.05250	0.00150	0.0000617	0.0000005	1.35	0.04	1.18	0.01	274.00	63.00	1.25	0.01
CBS-5a-5	3028	1887	1.6	0.001259	0.000027	0.0001837	0.0000009	5443.066	27.25681	0.05000	0.0011	0.0000622	0.0000004	1.28	0.03	1.18	0.01	171.00	46.00	1.26	0.01
CBS-5a-6	3780	1841	2.1	0.001331	0.000030	0.0001864	0.0000010	5365.958	28.50557	0.05170	0.0012	0.0000624	0.0000004	1.35	0.03	1.20	0.01	251.00	50.00	1.26	0.01
CBS-5a-7	1977	1501	1.3	0.001307	0.000034	0.0001865	0.0000011	5361.930	31.62533	0.05100	0.0014	0.0000633	0.0000006	1.33	0.04	1.20	0.01	207.00	57.00	1.28	0.01
CBS-5a-8	654.4	734	0.9	0.001350	0.000069	0.0001847	0.0000016	5414.185	46.90144	0.05280	0.0027	0.0000636	0.0000012	1.37	0.07	1.19	0.01	230.00	100.00	1.29	0.02
CBS-5a-9	1554	1363	1.1	0.001409	0.000043	0.0001865	0.0000017	5361.930	48.87550	0.05480	0.0018	0.0000644	0.0000008	1.43	0.04	1.20	0.01	365.00	71.00	1.30	0.02
CBS-5a-10	2761	1757	1.6	0.001303	0.000026	0.0001855	0.0000010	5390.254	27.89265	0.05070	0.0010	0.0000628	0.0000004	1.32	0.03	1.20	0.01	214.00	44.00	1.27	0.01
CBS-5a-11	3285	2139	1.5	0.001384	0.000036	0.0001856	0.0000011	5387.931	31.93278	0.05420	0.0014	0.0000631	0.0000005	1.41	0.04	1.20	0.01	355.00	60.00	1.28	0.01
CBS-5a-12	3640	2065	1.8	0.001282	0.000031	0.0001826	0.0000015	5476.451	44.98728	0.05100	0.0013	0.0000623	0.0000006	1.30	0.03	1.18	0.01	218.00	55.00	1.26	0.01
CBS-5a-13	2051	1457	1.4	0.001212	0.000034	0.0001829	0.0000012	5467.469	35.87185	0.04820	0.0014	0.0000628	0.0000006	1.23	0.03	1.18	0.01	88.00	58.00	1.27	0.01
CBS-5a-14	1662	1276	1.3	0.001261	0.000036	0.0001840	0.0000012	5434.783	35.44423	0.0500	0.0015	0.0000626	0.0000006	1.28	0.04	1.19	0.01	149.00	61.00	1.27	0.01
CBS-5a-15	1889	1348	1.4	0.001248	0.000043	0.0001827	0.0000015	5473.454	44.93804	0.04960	0.0017	0.0000619	0.0000006	1.27	0.04	1.18	0.01	144.00	73.00	1.25	0.01
Trachybasalt dike 2, CBS-6a, mean = 1.20 ± 0.0048 Ma, *n* = 10																					
CBS-6a-01	3104	1829	1.7	0.001326	0.000030	0.0001856	0.0000010	5387.060	28.7302100	0.05190	0.00120	0.0000638	0.0000005	1.35	0.03	1.20	0.01	250.00	50.00	1.29	0.01
CBS-6a-02	7090	3433	2.1	0.001266	0.000021	0.0001838	0.0000011	5440.696	32.5613000	0.05005	0.00085	0.0000614	0.0000004	1.29	0.02	1.18	0.01	182.00	37.00	1.24	0.01
CBS-6a-03	1268	1231	1.0	0.001359	0.000037	0.0001863	0.0000014	5367.687	40.3368800	0.05320	0.00150	0.0000653	0.0000007	1.38	0.04	1.20	0.01	285.00	59.00	1.32	0.02
CBS-6a-04	2543	1671	1.5	0.001272	0.000030	0.0001867	0.0000011	5356.186	31.5576100	0.04950	0.00120	0.0000632	0.0000005	1.29	0.03	1.20	0.01	144.00	50.00	1.28	0.01
CBS-6a-05	879	1073	0.8	0.001361	0.000044	0.0001854	0.0000013	5393.743	37.8202100	0.05330	0.00170	0.0000649	0.0000009	1.38	0.05	1.20	0.01	286.00	69.00	1.31	0.02
CBS-6a-06	1552	1229	1.3	0.001266	0.000046	0.0001861	0.0000015	5373.455	43.3110300	0.04950	0.00180	0.0000631	0.0000006	1.29	0.05	1.20	0.01	138.00	76.00	1.28	0.01
CBS-6a-07	1429	1139	1.3	0.001317	0.000046	0.0001854	0.0000015	5393.743	43.6387000	0.05140	0.00180	0.0000624	0.0000008	1.34	0.05	1.19	0.01	222.00	74.00	1.26	0.02
CBS-6a-08	1198	1218	1.0	0.001410	0.000041	0.0001852	0.0000013	5399.568	37.9019400	0.05530	0.00160	0.0000637	0.0000008	1.43	0.04	1.19	0.01	368.00	64.00	1.29	0.02
CBS-6a-09	2466	1577	1.6	0.001354	0.000034	0.0001863	0.0000011	5367.687	31.6932600	0.05290	0.00130	0.0000633	0.0000005	1.37	0.03	1.20	0.01	289.00	55.00	1.28	0.01
CBS-6a-10	4087	2573	1.6	0.001316	0.000025	0.0001874	0.0000010	5336.179	28.4748100	0.05100	0.00100	0.0000638	0.0000004	1.34	0.03	1.21	0.01	216.00	42.00	1.29	0.01

TABLE 2 | MC-LA-ICP-MS zircon Lu–Hf isotopic data for the trachybasalt dikes of the Changbai Mountain volcanic area.

No.	Age (Ma)	$^{176}Yb/^{177}Hf$	2σ	$^{176}Lu/^{177}Hf$	2σ	$^{176}Hf/^{177}Hf$	2σ	εHf(0)	εHf(t)	TDM1 (Ma)	TDM2 (Ma)	fLu/Hf
Trachybasalt dike 1, CBS-5a, *n* = 15												
CBS-5a-01	1.21	0.062707	0.001568	0.002052	0.000040	0.282700	0.000018	−2.6	−2.5	805	1768	−0.94
CBS-5a-02	1.21	0.055832	0.000777	0.001865	0.000028	0.282757	0.000017	−0.5	−0.5	719	1585	−0.94
CBS-5a-03	1.20	0.073038	0.000130	0.002444	0.000007	0.282764	0.000017	−0.3	−0.3	720	1562	−0.93
CBS-5a-04	1.18	0.038649	0.001056	0.001411	0.000035	0.282752	0.000017	−0.7	−0.7	718	1603	−0.96
CBS-5a-05	1.18	0.029207	0.000286	0.000992	0.000008	0.282720	0.000017	−1.8	−1.8	754	1702	−0.97
CBS-5a-06	1.20	0.050335	0.000730	0.001737	0.000023	0.282714	0.000015	−2.0	−2.0	778	1722	−0.95
CBS-5a-07	1.20	0.074336	0.001120	0.002543	0.000040	0.282722	0.000022	−1.8	−1.7	783	1696	−0.92
CBS-5a-08	1.19	0.050710	0.001263	0.001737	0.000046	0.282720	0.000016	−1.8	−1.8	769	1703	−0.95
CBS-5a-09	1.20	0.029297	0.000238	0.001044	0.000007	0.282720	0.000014	−1.8	−1.8	755	1703	−0.97
CBS-5a-10	1.20	0.080004	0.000779	0.002703	0.000026	0.282720	0.000018	−1.8	−1.8	790	1703	−0.92
CBS-5a-11	1.20	0.069372	0.000220	0.002339	0.000007	0.282762	0.000015	−0.4	−0.3	721	1570	−0.93
CBS-5a-12	1.18	0.016243	0.000180	0.000588	0.000006	0.282727	0.000014	−1.6	−1.6	736	1680	−0.98
CBS-5a-13	1.18	0.063841	0.000410	0.002154	0.000012	0.282741	0.000017	−1.1	−1.1	748	1638	−0.94
CBS-5a-14	1.19	0.062606	0.000248	0.002097	0.000011	0.282742	0.000016	−1.1	−1.0	745	1632	−0.94
CBS-5a-15	1.18	0.062604	0.000729	0.002075	0.000020	0.282755	0.000014	−0.6	−0.6	726	1593	−0.94
Trachybasalt dike 2, CBS-6a, *n* = 10												
CBS-6a-01	1.20	0.043957	0.000447	0.001522	0.000011	0.282731	0.000017	−1.5	−1.4	749	1668	−0.95
CBS-6a-02	1.18	0.017150	0.001408	0.003769	0.000035	0.282766	0.000015	−0.2	−0.2	745	1558	−0.89
CBS-6a-03	1.20	0.068196	0.001944	0.002352	0.000062	0.282729	0.000016	−1.5	−1.5	769	1674	−0.93
CBS-6a-04	1.20	0.072148	0.001162	0.002389	0.000043	0.282750	0.000020	−0.8	−0.8	740	1608	−0.93
CBS-6a-05	1.20	0.046462	0.000438	0.001613	0.000014	0.282729	0.000013	−1.5	−1.5	754	1674	−0.95
CBS-6a-06	1.20	0.031677	0.000113	0.001078	0.000004	0.282746	0.000014	−0.9	−0.9	720	1622	−0.97
CBS-6a-07	1.19	0.039444	0.000217	0.001324	0.000005	0.282745	0.000016	−0.9	−0.9	725	1622	−0.96
CBS-6a-08	1.19	0.038749	0.000527	0.001339	0.000016	0.282769	0.000013	−0.1	−0.1	692	1548	−0.96
CBS-6a-09	1.20	0.047389	0.000692	0.001586	0.000023	0.282750	0.000014	−0.8	−0.7	723	1607	−0.95
CBS-6a-10	1.21	0.085789	0.001011	0.002845	0.000033	0.282747	0.000017	−0.9	−0.9	754	1618	−0.91

quenched with air for 1 min to produce flat discs on the 5fire brick for the XRF analyses. Trace elements and rare earth elements (REEs) were analyzed by Perkin-Elmer ELAN 300D ICP-MS (United States). The detailed sample-digestion procedure refers to Sun et al. (2013). The analytical precisions for major elements and trace elements were better than 3 and 5%, respectively, and the major and trace element compositions of the trachybasalt dikes (CBS-5a, CBS-5b, CBS-5c, CBS-5a-1, CBS-5b-1, CBS-6a, and CBS-6b) are given in **Table 3**.

TABLE 3 | Major (wt%) and trace element (ppm) compositions of the trachybasalt dikes of the Changbai Mountain volcanic area.

Sample No.	Trachybasalt dyke 1			Trachybasalt dyke 2			
	CBS-5a	CBS-5b	CBS-5c	CBS-6a-1	CBS-6b-1	CBS-6a	CBS-6b
SiO_2	49.32	49.35	49.20	49.28	49.36	49.08	49.14
Al_2O_3	16.00	16.05	15.94	16.04	15.94	15.67	15.75
TiO_2	3.36	3.36	3.33	3.36	3.34	3.28	3.26
Fe_2O_3	13.79	13.85	13.75	13.86	13.72	13.70	13.65
FeO	7.19	7.01	7.15	7.08	7.11	5.17	7.35
TFe_2O_3	19.60	19.47	19.52	19.55	19.46	17.50	17.50
MnO	0.17	0.17	0.17	0.17	0.17	0.17	0.17
MgO	4.24	4.27	4.24	4.25	4.22	4.00	4.00
CaO	6.80	6.81	6.78	6.84	6.80	6.69	6.65
Na_2O	3.82	3.83	3.79	3.82	3.80	3.54	3.77
K_2O	2.55	2.54	2.55	2.51	2.51	2.34	2.45
P_2O_5	0.74	0.74	0.73	0.74	0.74	0.70	0.70
$K_2O + Na_2O$	6.37	6.38	6.34	6.34	6.31	5.88	6.22
LOI	−0.57	−0.54	−0.59	−0.68	−0.64	0.08	−0.28
Total	100.24	100.43	99.88	100.20	99.95	105.13	105.13
K_2O/Na_2O	0.67	0.66	0.67	0.66	0.66	0.66	0.65
A/CNK	1.21	1.22	1.21	1.22	1.22	1.25	1.22
Mg*	27.85	28.09	27.92	27.93	27.88	28.96	27.27
Li	3.53	3.52	3.74	3.63	3.63	3.62	3.72
Be	2.29	2.27	2.34	2.26	2.26	2.27	2.31
K	21167.87	21109.79	21159.57	20860.85	20811.06	20860.85	20811.06
P	3282.73	3273.85	3256.08	3287.18	3264.96	3287.18	3264.96
Sc	17.16	18.00	18.28	17.60	17.97	18.97	18.99
Ti	20768.96	20901.33	21122.11	21030.50	21379.13	19823.08	19716.12
V	227.44	229.28	232.56	231.29	232.57	229.28	232.56
Cr	7.66	7.88	7.76	7.58	7.80	7.88	7.79
Co	38.20	38.68	39.30	38.69	39.10	38.68	39.32
Ni	26.60	26.65	27.33	26.78	26.74	26.65	27.34
Cu	18.19	18.32	18.75	18.33	18.53	18.32	18.76
Zn	155.77	155.14	160.57	157.30	161.23	155.14	160.57
Ga	27.24	27.49	27.63	26.76	27.25	27.49	27.63
Rb	46.27	54.18	57.13	52.21	54.94	54.18	57.13
Sr	629.96	649.46	655.50	638.34	650.66	649.46	655.50
Zr	310.96	311.58	317.01	313.45	312.83	311.58	317.01
Nb	49.05	49.30	50.20	49.49	49.27	49.30	50.20
Mo	2.15	2.13	2.17	2.11	2.12	2.13	2.17
Cd	0.30	0.29	0.30	0.29	0.29	0.29	0.30
In	0.10	0.10	0.09	0.10	0.10	0.10	0.09
Sb	0.05	0.04	0.05	0.04	0.05	0.04	0.05
Cs	0.34	0.35	0.36	0.35	0.33	0.35	0.36
Ba	767.78	798.94	813.59	776.41	807.94	798.94	812.59
Hf	7.42	7.41	7.43	7.35	7.57	7.41	7.52
Ta	2.99	2.95	2.96	2.91	3.00	2.95	2.97
W	0.94	0.90	0.90	0.90	0.92	0.90	0.91
Tl	0.03	0.03	0.03	0.03	0.03	0.03	0.29
Pb	6.49	7.37	7.77	6.82	7.62	7.37	7.76
Bi	0.01	0.01	0.01	0.00	0.01	0.01	0.01
Th	5.15	5.13	5.16	5.02	5.30	5.13	5.22
U	1.13	1.12	1.14	1.11	1.16	1.12	1.15
Y	34.17	34.22	34.78	34.18	34.62	34.22	34.68
La	45.38	46.23	46.96	45.23	46.86	46.23	46.86
Ce	93.81	94.12	95.39	92.97	95.57	94.12	95.40
Pr	11.36	11.41	11.61	11.22	11.65	11.41	11.61
Nd	45.91	45.99	46.54	45.13	46.90	45.99	46.56
Sm	9.77	9.70	9.84	9.53	9.92	9.77	9.88
Eu	3.00	2.98	3.00	2.93	3.05	2.93	3.04
Gd	8.98	8.94	9.01	8.82	9.09	8.80	9.07
Tb	1.28	1.27	1.28	1.25	1.29	1.27	1.28
Dy	6.78	6.72	6.80	6.64	6.89	6.66	6.88
Ho	1.29	1.28	1.30	1.26	1.32	1.26	1.32
Er	3.25	3.23	3.24	3.17	3.31	3.17	3.31
Tm	0.45	0.44	0.45	0.43	0.45	0.43	0.45
Yb	2.66	2.65	2.67	2.60	2.72	2.75	2.73

(Continued on following page)

TABLE 3 | (*Continued*) Major (wt%) and trace element (ppm) compositions of the trachybasalt dikes of the Changbai Mountain volcanic area.

Sample No.	Trachybasalt dyke 1			Trachybasalt dyke 2			
	CBS-5a	CBS-5b	CBS-5c	CBS-6a-1	CBS-6b-1	CBS-6a	CBS-6b
Lu	0.40	0.40	0.40	0.39	0.41	0.40	0.42
ΣREE	234.31	235.36	238.47	231.56	239.43	284.78	297.78
LREE	209.23	210.43	213.33	207.01	213.96	265.66	273.66
HREE	25.08	24.93	25.14	24.56	25.47	24.72	25.48
LREE/HREE	8.34	8.44	8.48	8.43	8.40	8.51	8.37
La_N/Yb_N	11.49	11.75	11.87	11.71	11.63	11.35	11.61
δEu	0.96	0.96	0.96	0.96	0.97	0.95	0.98
δCe	0.97	0.96	0.96	0.97	0.96	0.96	0.96
$(Na_2O + K_2O)/δEu$	6.61	6.63	6.62	6.60	6.52	6.70	6.64

**Mg (Magnesium index) = mole [100 * (MgO/40.3044)/(MgO/40.3044 + (FeO + Fe2O3 * 0.8998)/71.844)].*

TABLE 4 | Lead isotope compositions of trachybasalt dikes in the study area.

Sample No.	$^{206}Pb/^{204}b$	1σ	$^{207}Pb/^{204}Pb$	1σ	$^{208}Pb/^{204}Pb$	1σ	$^{207}Pb/^{206}Pb$	1σ	$^{208}Pb/^{206}Pb$	1σ
CBS-5a-1	17.7047	0.00024	15.5525	0.00020	38.0870	0.00069	0.8788	0.00001	2.1517	0.00003
CBS-5b-1	17.7164	0.00018	15.5549	0.00016	38.0933	0.00063	0.8786	0.00001	2.1512	0.00003
CBS-5c-1	17.7241	0.00026	15.5580	0.00021	38.0929	0.00058	0.8784	0.00001	2.1502	0.00002
CBS-6a-1	17.7071	0.00084	15.5553	0.00029	38.0958	0.00098	0.8791	0.00003	2.1525	0.00008
CBS-6b-1	17.7172	0.00025	15.5564	0.00023	38.0993	0.00076	0.8786	0.00001	2.1514	0.00003

Sr-Nd-Pb Isotopic Analyses

Whole-rock Pb isotopic measurements were conducted by a MAT-261 thermal ionization mass spectrometer. All chemical preparations were performed on class 100 work benches within a class 1000 over-pressured clean laboratory. Sample digestion is as follows: 1) sample powder (200 mesh) was placed in an oven at 105°C for drying of 12 h; 2) 50–200 mg sample powder was accurately weighed and placed in a Teflon bomb; 3) 1–3 ml HNO_3 and 1–3 ml HF were added into the Teflon bomb; 4) Teflon bomb was put in a stainless steel pressure jacket and heated to 190 °C in an oven for >24 h; 5) after cooling, the Teflon bomb was opened and placed on a hotplate at 140°C and evaporated to incipient dryness, and then 1 ml HNO3 was added and evaporated to dryness again; and 6) the sample was dissolved in 1.0 ml of 1.0 M HBr. After centrifugation, the supernatant solution was loaded into an ion-exchange column packed with AG resin. After complete draining of the sample solution, columns were rinsed with 1.0 M HBr to remove undesirable matrix elements. Finally, the Pb fraction was eluted using 6.0 M HCl and gently evaporated to dryness prior to mass-spectrometric measurement. The sample analyses were performed at the Analytical Laboratory of the Beijing Research Institute of Uranium Geology (BRIUG), the precision of $^{20x}Pb/^{204}Pb$ is (0.002–0.025%, 1σ), and the accuracy is better than 0.03%. The results of the whole-rock Pb isotopic analyses are given in **Table 4**.

The results of Sr–Nd isotope analyses are reported in **Table 5**. All chemical preparations were performed on class 100 work benches within a class 1000 over-pressured clean laboratory; the experimental process refers to Pan et al. (2020). The REE solution was used to separate the Nd fraction by the Nd-column method. Sr and Nd isotopes analyses were performed on a Nu Plasma II MC-ICP-MS (Wrexham, Wales, UK) at the Analytical Laboratory of the BRIUG, Beijing, China. The precision of the test sample = 0.000005–0.00002 (0.01–0.05‰, 1σ), better than 0.000025 (~0.05‰). Raw data of isotopic ratios were corrected for mass fractionation by normalizing to $^{86}Sr/^{88}Sr = 0.1194$ for Sr, $^{146}Nd/^{144}Nd = 0.7219$ for Nd, and $^{205}Tl/^{203}Tl = 2.3885$ for Pb with exponential law. International isotopic standards (NIST SRM 987 for Sr, JNdi-1 for Nd, and NIST SRM 981 for Pb) were periodically analyzed to correct instrumental drift. Geochemical reference materials of USGS BCR-2, BHVO-2, AVG-2, and RGM-2 were treated as quality control.

RESULTS

Zircon U–Pb Dating

Zircons from the trachybasalt dikes (sample CBS-5a and CBS-6a) are light gray with no inclusions. They are euhedral–subhedral columnar crystals with size of 50–200 μm (aspect ratio of 1:1 to 3:1). In cathodoluminescence (CL) images, the zircons exhibit low, homogeneous luminescence and occasionally display oscillatory zoning (**Figure 4**). Th/U is 0.8–2.5, a range of values consistent with a magmatic origin (Hoskin and Schaltegger, 2003). The 25 analyses of zircon grains from CBS-5a and CBS-6a give weighted mean $^{206}Pb/^{238}U$ ages of 1.19 ± 0.0057 Ma (MSWD = 2.00, *n* = 015) and 1.20 ± 0.0048 Ma (MSWD = 0.89, *n* = 10), respectively (**Figures**

TABLE 5 | Sr–Nd isotopic data of trachybasalt dikes in the study area.

Sample No.	t	Rb	Sr	$^{87}Rb/^{86}Sr$	$^{87}Sr/^{86}Sr$	1σ	$^{84}Sr/^{86}Sr$	1σ	$(^{87}Sr/^{86}Sr)i$	Sm	Nd	$^{147}Sm/^{144}Nd$	$^{143}Nd/^{144}Nd$	1σ	$(^{143}Nd/^{144}Nd)i$	εNd(t)	TDM1	TDM2	fSm/Nd
	Ma	ppm	ppm							ppm	ppm						Ma	Ma	
CBS-5a-1	1.19	46.27	629.96	0.207480	0.705328	0.000006	0.006783	0.000001	0.056809	0.000008	0.705324	9.77	45.91	0.133612	0.512553	0.000006	0.512552	−1.65	1139	953	−0.32
CBS-5b-1	1.19	54.18	649.46	0.235616	0.705290	0.000005	0.006780	0.000001	0.056786	0.000007	0.705286	9.70	45.99	0.132364	0.512567	0.000005	0.512566	−1.37	1095	931	−0.33
CBS-5c-1	1.19	57.13	655.50	0.246157	0.705269	0.000006	0.006781	0.000001	0.056792	0.000008	0.705264	9.84	46.54	0.132682	0.512572	0.000004	0.512571	−1.28	1091	924	−0.33
CBS-6a-1	1.20	52.21	638.34	0.231031	0.705240	0.000004	0.006804	0.000001	0.056984	0.000007	0.705236	9.53	45.13	0.132496	0.512608	0.000003	0.512607	−0.58	1021	867	−0.33
CBS-6b-1	1.20	54.94	650.66	0.238499	0.705169	0.000005	0.006803	0.000001	0.056974	0.000006	0.705165	9.92	46.90	0.132773	0.512581	0.000004	0.512580	−1.10	1075	910	−0.32

Note: the initial ratio of Sr–Nd isotopes and the model age are based on λRb = 1.43 × 10–11 years–1and λSm = 6.540 × 10–12 years–1 (Peucat et al., 1988).

5B,D). Because the magmatism in the Tianchi area occurred in the late Cenozoic, the content of common Th, U, and Pb in the Th-U-Pb system of zircons may be considered high, and the content of ^{235}U decays to ^{207}Pb is low. Therefore, $^{206}Pb/^{208}U$ is selected as the weighted average age. Tera-Wasserburg concordia diagrams were used to calculate the concordant age (1.19 ± 0.0030 Ma and 1.20 ± 0.0038, respectively, **Figures 5A,C**). This age is taken to represent the emplacement age of the studied dikes.

Zircon Lu–Hf Isotopic Data

The spots used for LA-MC-ICP-MS U–Pb dating are the same as those for *in situ* zircon Lu–Hf isotopic analysis. Twenty-five analyses of the trachybasalt dikes (sample CBS-5a and CBS-6a) yielded $^{176}Hf/^{177}Hf$ of 0.282700–0.282769, εHf(t) = −2.5 to −0.1, and T_{DM2} = 1548–1768 Ma (**Figure 8A**).

Whole-Rock Geochemistry

The dikes show a trachybasaltic composition (SiO_2 = 49.08–49.35 wt%; Na_2O = 3.54–3.83 wt%, and K_2O = 2.34–2.55 wt%) with high Al_2O_3 (15.67–16.05 wt%) and P_2O_5 (0.70–0.74 wt%) contents and have a potassic affinity (**Figures 6A,B**). Mantle-normalized trace element (REE) and chondrite-normalized rare earth element patterns are reported in **Figures 7A,B**. The samples display parallel trace element patterns. They show relative enrichments in LILE and HSFE. The Zr/Nb (6.31–6.35), La/Nb (0.91–0.95), Ba/Nb (15.65–16.21), Ba/Th (149.22–157.57), Rb/Nb (0.94–1.14), K/Nb (421.50–431.55), Th/Nb (0.10–0.11), and Ba/La (16.92–17.33) values are higher than those of MORB, whereas the chondrite-normalized REEs show enrichments in LREE and depletion in HREE; LREE/HREE ranges from 8.34 to 8.48. The dikes are characterized by a low differentiated REE pattern (La_N/Yb_N = 11.49–11.75) and weak Eu negative anomalies (Eu/Eu* = δEu = 0.96–0.97).

Lead Isotope Composition

The dikes have moderately high $^{206}Pb/^{204}Pb$ (17.7047–17.7241) values with $^{207}Pb/^{204}Pb$ = 15.5525–15.5580 and $^{208}Pb/^{204}Pb$ = 38.0870–38.0993. In the $^{207}Pb/^{204}Pb$ vs. $^{206}Pb/^{204}Pb$ plots (**Figure 8B**), they lie within or close to the values representative of the lower crust.

Sr–Nd Isotope Composition

Five samples of the trachybasalt dikes were analyzed for their whole-rock Sr–Nd isotopic composition. They have evolved radiogenic isotope compositions with $(^{87}Sr/^{86}Sr)_i$ = 0.705165–0.705324 and $(^{143}Nd/^{144}Nd)_i$ = 0.512552–0.512607 corresponding to εNd (t) values of −0.58 to −1.65. According to the data reported in **Figure 8C**, the Sr–Nd isotope composition of the trachybasaltic dikes approaches that of the coeval basaltic rocks in the CMVF region.

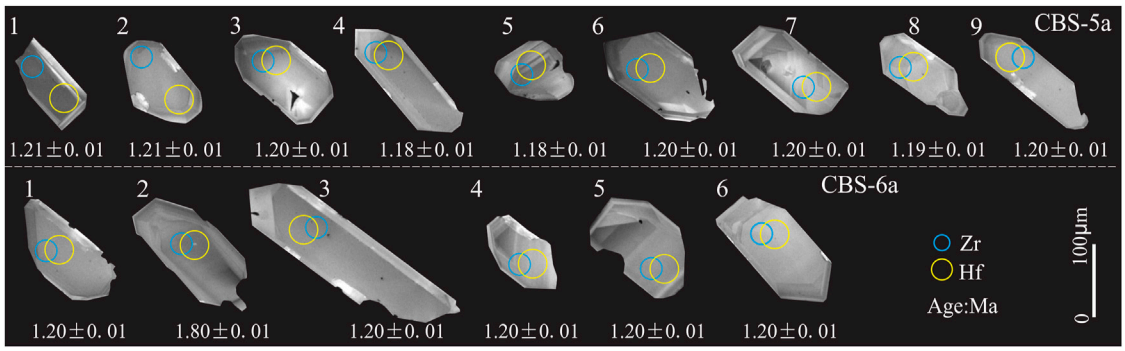

FIGURE 4 | Cathodoluminescence (CL) images of zircons from the trachybasalt dike.

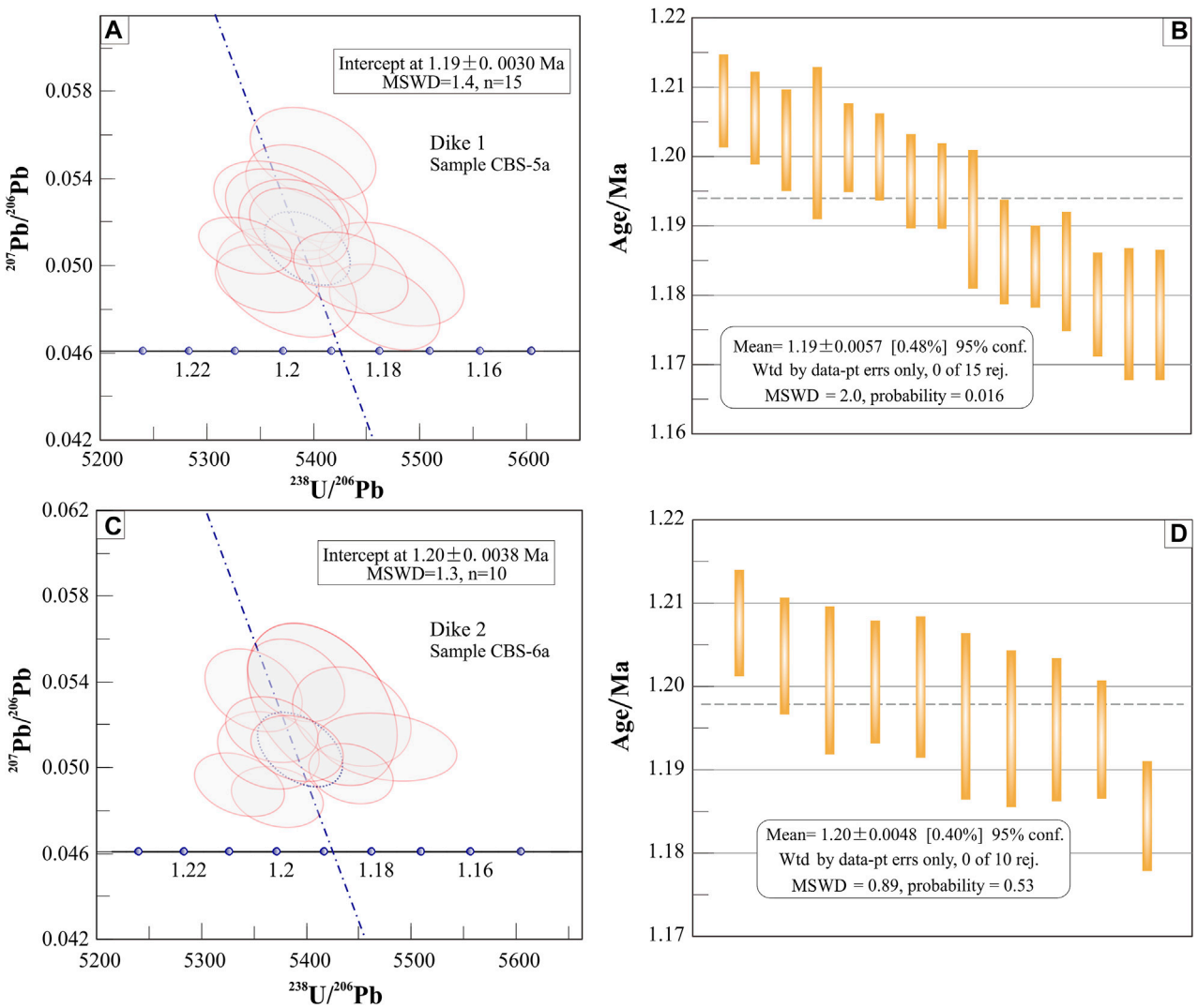

FIGURE 5 | (A, B) Tera–Wasserburg concordia diagram for individual zircons determined by LA-MC-ICP-MS from the trachybasalt dike; **(C, D)** $^{206}Pb/^{208}Pb$ weighted average age of zircons.

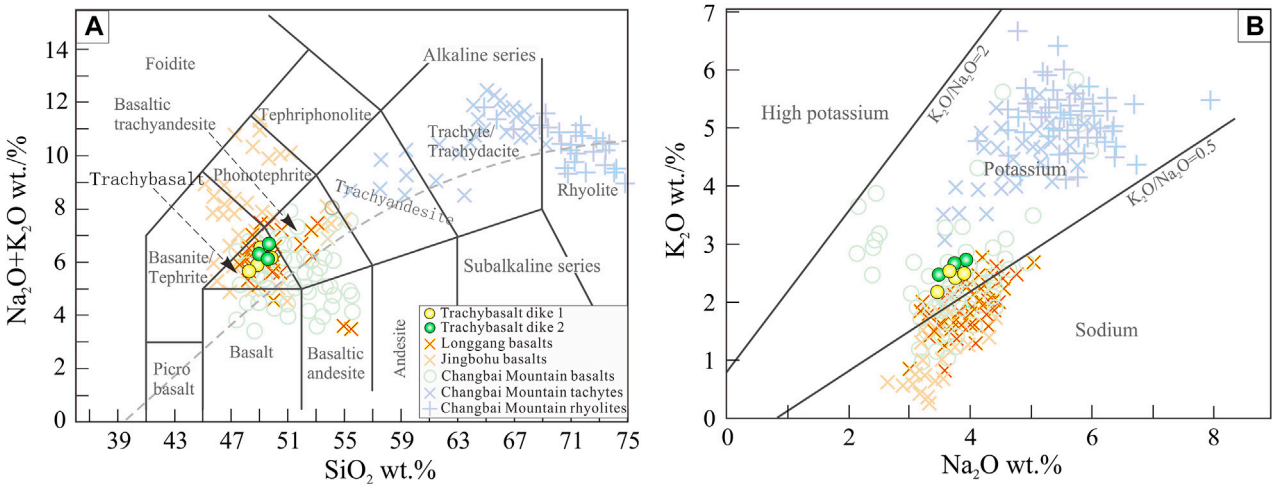

FIGURE 6 | (A) TAS (Le Maitre, 1989) and **(B)** K_2O vs. Na_2O diagrams of Middlemost (1994) showing the classification of the trachybasaltic dikes. Other data are from Wei (2014), Ma et al. (2015), Lei et al. (2020), Andreeva et al. (2014), Liu et al. (2015), and Zhang et al. (2015).

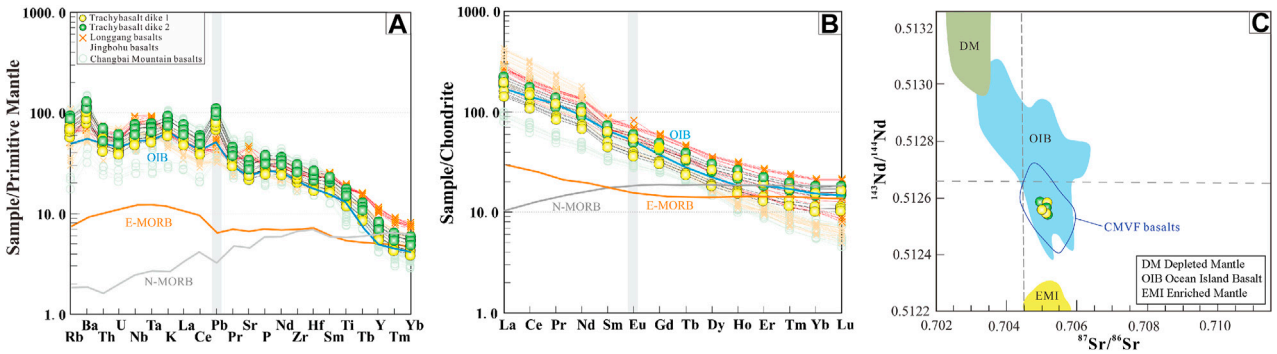

FIGURE 7 | (A) Normalized REE patterns and **(B)** trace element spidergrams for the trachybasaltic dike and trachybasalts in the region (Boynton, 1984; Sun and McDonough, 1989). Other data sources are as for **Figure 7C**; $^{143}Nd/^{144}Nd$ versus $^{87}Sr/^{86}Sr$ plot of the CMVF trachybasalts. The field of the Changbaishan basalts is from Zhang et al. (2018). Reference ranges for DM, enriched mantle (EM1 and EM2), MORB, and OIB are from Zindler and Hart (1986).

DISCUSSION

Timing and Tectonic Control of Volcanism at CMVF

Application of U–Pb disequilibrium dating of zircons with contrasting stabilities and compositions can provide a unique perspective to study the evolution of magma within the framework of absolute time (Wu et al., 2004). All dike outcrops in the field consist of hypabyssal basalts (**Figures 3A,B**). All dated zircons from the dikes are euhedral–subhedral columnar crystals and display oscillatory zoning; their Th/U is 0.8–2.5, a value consistent with a magmatic origin. Although the zircon crystals of the two dikes could be interpreted as antecrysts, however, their petrographic features do not support such hypothesis. The growth of zircons in poorly evolved magmas may be due to different processes including (Borisova et al., 2020) the partial melting of hydrated peridotite, the felsic crustal involvement/recycling or zircon sealing, total zircon dissolution, and reprecipitation and/or a contribution of metasomatic Si-F-rich fluid. Our data do not allow us to better constrain the origin of the CMVF zircons studied here. As preliminary hypothesis, crustal recycling (see Discussion) or metasomatic processes in a hypabyssal environment could be responsible for the formation of the zircon crystals of CMVF dikes. Field observations suggest that dikes were formed by basaltic magma hypabyssal process (**Figures 3A,B**), consistent with the euhedral–subhedral columnar morphology and oscillatory zoning of all the dated zircon crystals. Single grain LA-MC-ICP-MS zircon U–Pb concordance ages of 1.19–1.20 Ma (n = 25) and $^{206}Pb/^{238}U$ ages (1.18–1.20 Ma) are here obtained from the trachybasaltic dikes and confirm that the age is 1.18–1.20 Ma. We conclude that studied dikes emplaced in the Calabrian stage of Pleistocene. As previously reported, the last three main stages of the Tianchi

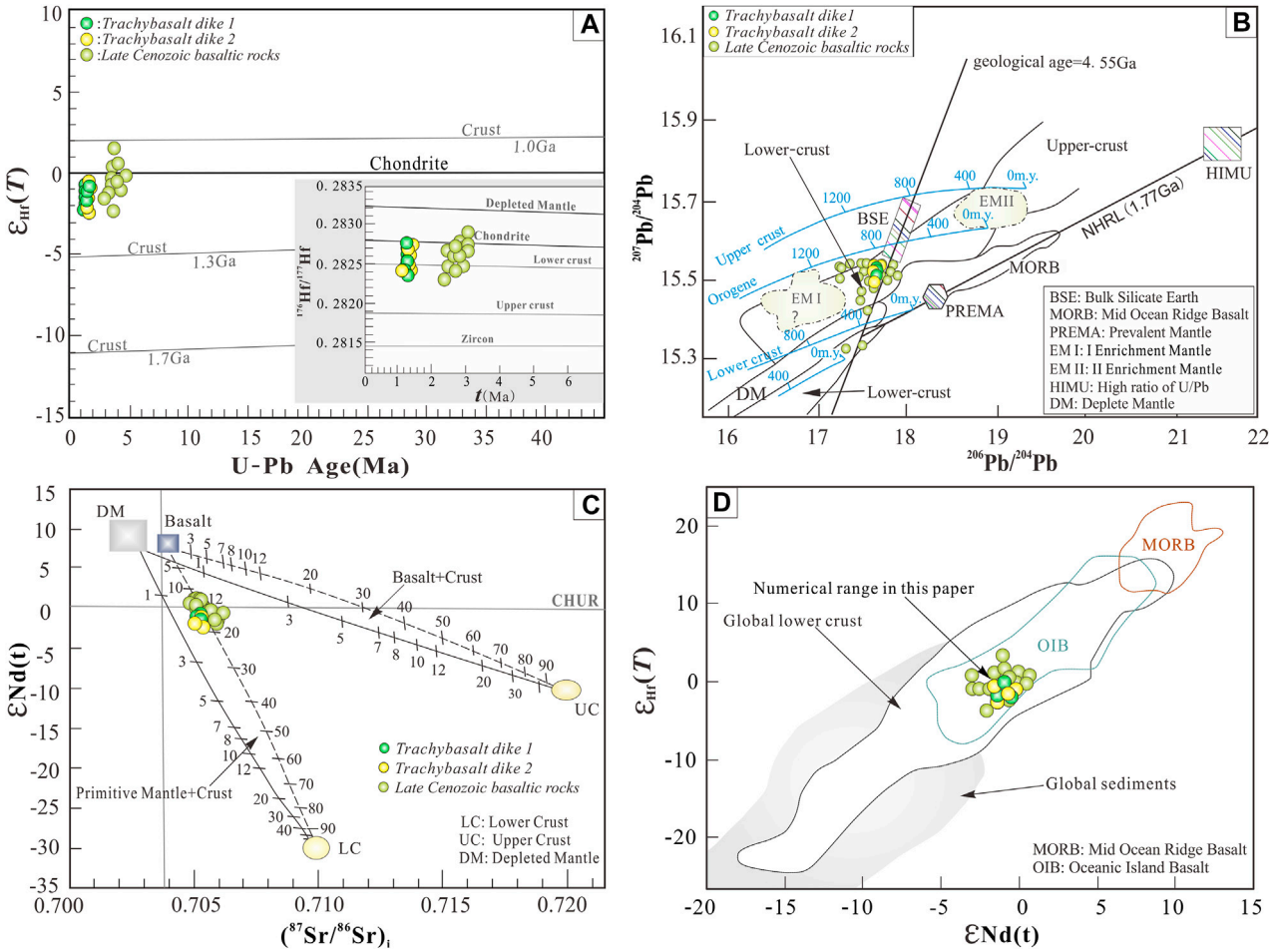

FIGURE 8 | (A) U-Pb age vs. εHf(t) of zircon diagram (after Bizzarro et al., 2002; Wu et al., 2007; Zou et al., 2008); **(B)** $^{207}Pb/^{204}Pb$ vs. $^{206}Pb/^{204}Pb$ diagram (after Zartman and Doe 1981); **(C)** εNd(t) vs. $(^{87}Sr/^{86}Sr)_i$ diagram (after Wu et al., 2002; Sun et al., 2014; Wang et al., 2017); the modeling results of assimilation of lower and upper crust material by DM and basaltic melts are reported as black lines; the fractions (in %) of assimilated crustal material are reported as tick marks; **(D)** εHf(t) vs. εNd(t) diagram (diagram modified after Dobosi et al., 2003 and Zhu, 2007). Other data sources are as for **Figure 7**.

volcanism are 2.8–0.3 Ma (shield stage), 1.5–0.01 Ma (cone construction stage), and 0.2 Ma-present (caldera-forming stage) (Cheong et al., 2019; Zou et al., 2021). Therefore, our new geochronological data show that the trachybasalt dikes emplaced between the shield and cone forming stages (**Figures 9A-C**). The trachybasalt dikes, which are coeval with the less evolved basaltic magmatism, evidence an early phase of evolution processes within the CMVF magmatic system, at least in the Tianchi norther sector. Our field data better constrain the role of regional tectonics in controlling the CMVF volcanism during Calabrian. In fact, the NW-SE strike of dikes mirrors that of the major structural discontinuity affecting the CMVF area, i.e., the Baishan-Jince fault, and the preferred alignment of the monogenetic volcanoes (**Figure 1**). As a result, the CVMF Calabrian magmatism developed along a deep discontinuity probably affecting the whole crust along which basaltic magma upwelled and partly differentiated. The SiO_2 content and the values of A/CNK, MgO, Fe_2O_3, TiO_2, P_2O_5, and V of the dikes confirm that they represent poorly evolved products of mantle melts.

Petrogenesis

As known, intraplate magmatism can be due to different processes including 1) asthenosphere upwelling carried by mantle plume associated or not to a hot spot, 2) lithosphere thinning, continental stretching, and consequent upwelling of the lithospheric mantle, 3) fluid release from a subducting plate and mantle metasomatism, and 4) crust-mantle interaction (Defant and Drummond., 1990; Puffer, 2001; Sisson et al., 2005). The Sr, Nd, Pb, and Hf isotopic rations (**Figure 7C**; **Figures 8B,D**), Zr/Hf (41.35–42.69), Nb/Ta (16.41–16.98), Th/U (4.53–4.56), Th/La (0.11), Nb/U (43.49–44.58), and Lu/Hf (0.05), and the ratio of other trace elements (**Figure 7A,B**; **Figure 8**; Zhao, 2016) of the Calabrian CVMF dikes (**Figure 8B**) are consistent with an OIB-type mantle source (**Figure 10B**). In particular, the values of the Sr and Nd isotopic ratios (**Figure 7C**) overlap those of the CVMF basaltic rocks, for which an OIB source has been recognized (Zhang et al., 2018; Choi et al., 2020). However, the trace element pattern indicates that the source is more complex. The $(Na_2O + K_2O)/\delta Eu$ (6.52–6.63), Nb/La (1.05–1.09), La/Yb (10.36–17.61), Th/Nd (0.11–0.15), and δCe (0.96–0.97) values and incompatible

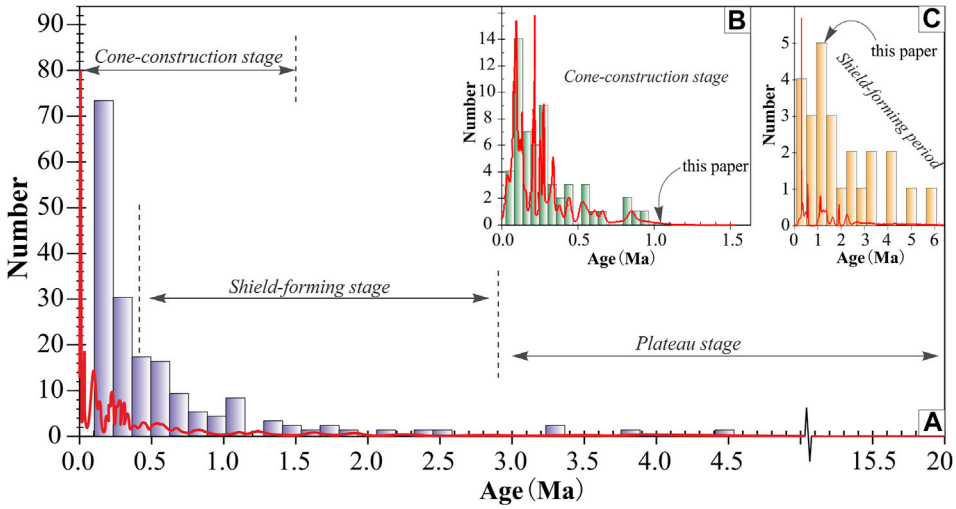

FIGURE 9 | (A) A summary of ages of the late Cenozoic volcanic rocks in the Changbai Mountain volcanic area and adjacent areas (e.g., Fan et al., 1999; Nakamura et al., 2000); **(B)** age frequency diagram of volcanic rocks during the cone construction stage in the Changbaishan Mountains volcanic area (e.g., Liu, 1981, 2015; Wang et al., 1999, 2001); **(C)** age frequency diagram of volcanic rocks during the shield-forming stage (other data sources are as for **Figure 7**).

trace element abundances such as Th, U, Nb, and Ta suggest the involvement of an enriched mantle type I (EMI) (**Figures 10C,D**) and some interactions with crustal material (**Figure 10A**). The CVMF Pleistocene basaltic rocks consist of early sodium-rich rocks to later potassic rocks, and the data obtained in this study indeed indicate an alkaline potassic affinity of the rocks emplaced during Calabrian. According to Wang et al. (2017) and Lei et al. (2020), the EMI signature of the NE China potassic volcanism could be due to fluids released by the Pacific sediments of the subducted Pacific slab. More in general, potassic rocks as those studied here are generally considered to be derived from the partial melting of a mantle modified by slab-derived fluids or melts from the subcontinental lithospheric mantle (SCLM) (Foley and Peccerillo, 1992). The last stage of the Pacific subduction plate between NE China and Japan may favor the dehydration of the oceanic crust allowing the partial melting of the mantle. In this framework, the interaction between hydrous fluid and the mantle can produce a phlogopite-bearing source whose partial melting may produce potassic magmas (Wyllie and Sekine, 1982; Condamine and Médard, 2014). Generally, melts in equilibrium with phlogopite are expected to have higher Rb/Sr (>0.1) and lower Ba/Rb (<20) values than those formed from amphibole-bearing mantle sources (Furman and Graham, 1999), and the early Pleistocene basaltic rocks of the study area have low Rb/Sr (0.07–0.09) and Ba/Rb (14.24–16.59) values. This suggests that potassic amphibole is the main K-rich phase. Because the mantle material is depleted of Zr and Hf, it is impossible for the mantle derived magma to crystallize zircon without the addition of crustal material. As a result, the occurrence of zircon in the mantle derived magma indicates that some crust-mantle interactions occurred during the magma emplacement (Zheng et al., 2006). The studied trachybasaltic dikes are characterized by negative εHf(t) values (−0.1 to −2.5), $^{176}Hf/^{177}Hf$ = 0.000588–0.003769, and the Mesoproterozoic two-stage Hf model ages are from 1548 Ma to 1768 Ma (**Figure 6A**). This indicates that there is some crustal material involved in the magma generation processes, i.e., crustal contamination. On the other hand, the consistent negative Nd isotopic compositions (εNd(t) = −0.58 to −1.67) of the trachybasalt dikes preclude their derivation from the melting of an old lower continental crust (T_{DM1} = 1021–1139 Ma). The variation ranges of the $(^{87}Sr/^{87}Sr)_I$ and εNd(t) values in the mafic rocks in the region are 0.70485–0.70619 and +0.02 to −1.65, respectively. These values indicate an initial magmatic source consisting of OIB-EMI type melts (**Figure 8C**). Furthermore, the Pb-Pb isotopic data (**Figure 8B**) of the trachybasalt dikes and CVMF basaltic rocks support a mixed source consisting of mantle and ancient lower crust components. In the εHf(t)-εNd(t) diagram (**Figure 8D**), all the samples fall into the overlapping area of the global lower crust and OIB. The results of the modeling of assimilation of lower crust material in **Figure 8C** suggest that the studied trachybasalts assimilated about 10–20% of crustal material.

Geodynamic Implications

The late Cenozoic basaltic rocks in the NE China continental margin have geochemical compositions consistent with OIB-type and EMI sources (Zhou and Armstrong, 1982; Xu et al., 2005; Zhi et al., 1990; Liu et al., 2015; Wang et al., 2015; Mao and Wang, 2000; Liu et al., 2008; Chen et al., 2009; Andreeva et al., 2014; Zhang et al., 2009; Ge et al., 2001; Wang et al., 2011). However, the CMVF Calabrian dikes studied here have moderate $Mg^{\#}$ (27.85–28.09) and higher Na_2O and K_2O contents with respect to the less evolved CMVF basaltic rocks (**Figure 6**). Therefore, the dikes do not represent primary magmas and experienced some crystal fractionation. Despite these features, they show geochemical features, e.g., values of Na_2O/K_2O and isotopic ratios, and some trace element contents, comparable with

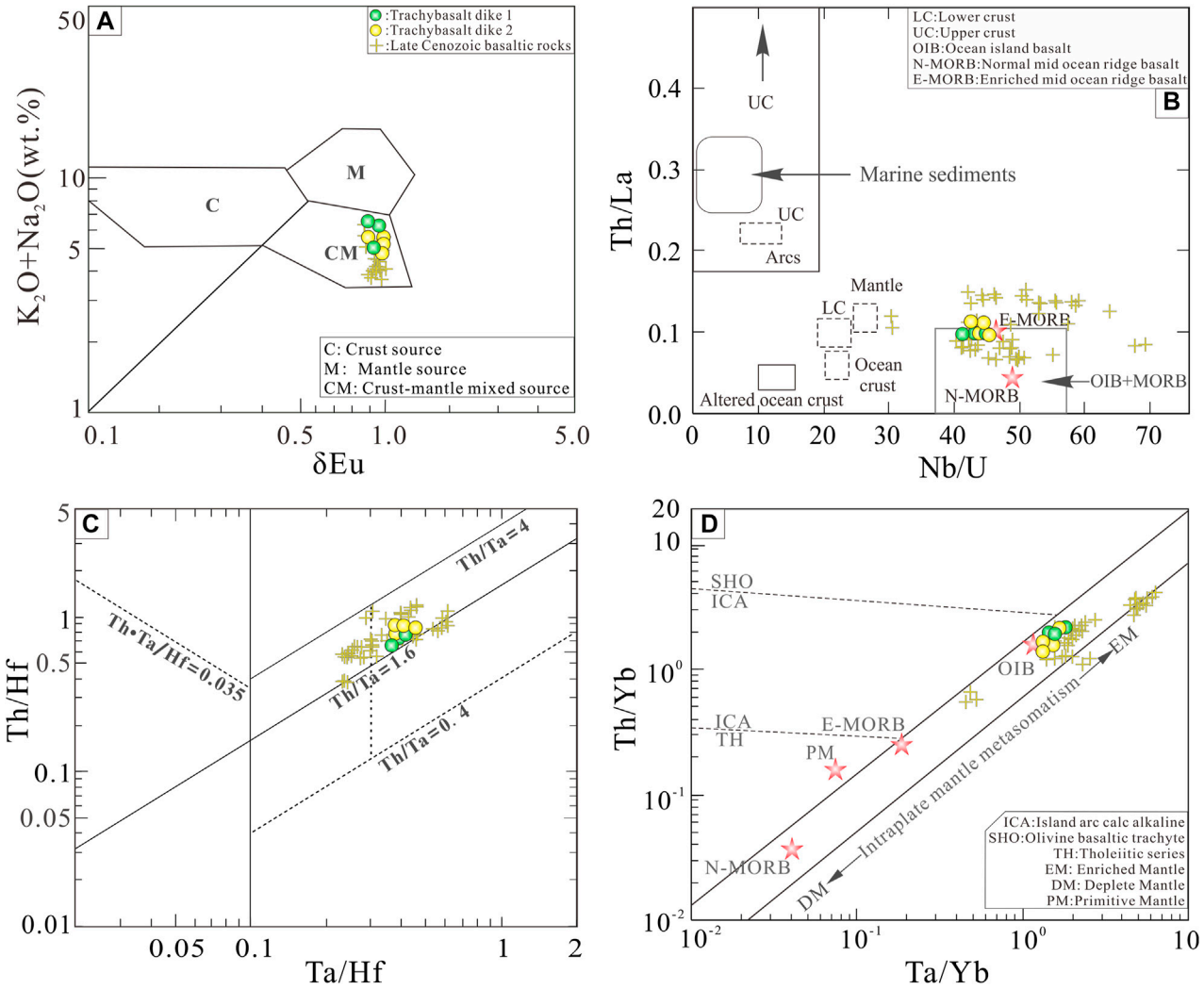

FIGURE 10 | (A) $K_2O + Na_2O$ vs. δEu, **(B)** Th/La vs. Nb/U, **(C)** Th/Hf vs. Ta/Hf, and **(D)** Th/Yb vs. Ta/Yb diagrams (Li, 1992; Deng, 2004; Zhao, 2016), showing that the eastern Jilin Province basaltic rocks (early Pleistocene, including the Changbai Mountain trachybasaltic dikes) mainly plot in the intraplate field. Data of the trachybasalt dikes are from this study, and other data sources are as for **Figure 7**.

those of the CMVF less evolved rocks (**Figure 6**, **Figure 7B**, and **Figures 8B–D**). This allows us to discuss the significance of the OIB and EMI signatures of the Pleistocene studied dike in the intraplate geodynamic context of NE China. Seismic tomography studies show that there is a high velocity anomaly in the mantle transition zone (MTZ) below NE China at 410–660 km depth, which is interpreted as the slab of the Pacific plate in the MTZ, and a low velocity body above the flat portion of the slab interpreted as a big mantle wedge (BMW) (Li and Hilst, 2010; Tian et al., 2016; Wang et al., 2020). From the middle Cenozoic, the subducted plate gradually subsided into the MTZ and partly melts. The resulting water-rich melt and the slab-derived fluids may metasomatize the overlying mantle. However, the EMI signature of the studied CMVF dikes cannot be explained by slab-derived sediments and associated metasomatizing fluids (Xu et al., 2012) because of their moderate Sr and low Pb isotopic ratios. In accordance with the geochemical signature of the gas emitted in NE China (Xu S. et al., 2013b) and of the Cenozoic basalts (Zhang et al., 2009), the EM1 source could be the subcontinental lithospheric mantle (SCLM) (**Figure 10D**; Zhu et al., 2011). Regarding the source of the late Cenozoic initial OIB magma in the continental margin of NE China, this source could be a response to the back-arc extension and rifting caused by the roll-back of the Pacific plate (Li and Hilst, 2010; Zheng et al., 2018). Some geophysical studies suggest, however, that the Pacific slab is broken and an OIB-type mantle plume upwells from the lower mantle crossing the slab and entering MTZ (Tang et al., 2014). This model is not supported by shear-wave splitting studies (Lynner and Long, 2014) which show trench-parallel sub-slab fast splitting directions and not, as expected for a mantle plume from the lower mantle, a vertical direction. Based on geochemical data, Kuritani et al. (2009) propose that a back-arc type rifting associated to the slab retreat and

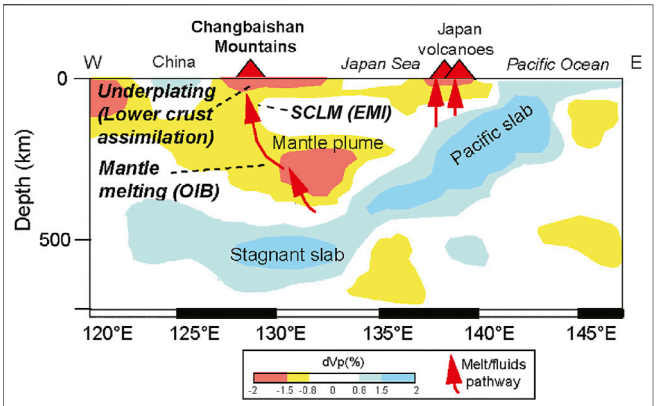

FIGURE 11 | Schematic model for the Pleistocene trachybasaltic volcanism of Changbaishan Mountains in NE China along a W-E striking section extending from NE China to Japan. Tomography (dVp%) is simplified from Ma et al. (2019). The depth of the OIB source, its EMI component, and the assimilation of crustal material are inferred for the large-scale structures evidenced from the tomography.

progressive flattening may favor the decompression melting of the asthenosphere. This model could explain the OIB signature of the CMVF basalts including the trachybasaltic dikes studied here. In this scenario, the CMVF OIB melts upwell from the asthenosphere to the lithosphere, where they mix to SCLM melts. These melts accumulate at the base of the lower crust in the early Pleistocene, where they may assimilate lower crust material of the ancient Asia continent (**Figure 8A** and **Figure 10A**). However, assimilation processes could affect the mantle melts during their upwelling and storage in the crust. Tomographic data in NE China (Zhu et al., 2019) clearly show a thickening of the Moho due to the accumulation of mantle melts at the base of the crust below CMVF. These data suggest active underplating process where these mantle melts may promote the melting of the lower crust. Therefore, we propose that most of the assimilation of crustal material underwent by the CMVF trachybasalts occurs at the Moho depth and not during their ascent and storage in the crust.

CONCLUSION

Out results indicate that trachybasaltic dikes emplaced in the Calabrian stage of Pleistocene at 1.19–1.20 Ma, i.e., in a time period marked by the transition from a monogenetic-type volcanism to the Tianchi cone construction, central-type activity. The Calabrian volcanism is associated to the emplacement of scoria cones whose shallower feeding systems are controlled by regional tectonics and, in particular, by NW-SE striking structures. Geochemical and Sr-Nd-Pb-Hf isotopic data show that the trachybasaltic dikes have a potassic affinity and their parental magma is constituted by an OIB-type asthenospheric source with an EM I signature related to SCLM melts associated to back-arc and rifting processes linked the slab retreat (**Figure 11**). The magma upraising from the mantle stops at the Moho and assimilates Mesoproterozoic lower crust material by underplating (**Figure 11**).

DATA AVAILABILITY STATEMENT

The original contributions presented in the study are included in the article; further inquiries can be directed to the corresponding author.

AUTHOR CONTRIBUTIONS

ML: formal analysis, and writing-original draft. ZX: investigation and data curation. GV: writing-review and editing. XP: project administration and formal analysis. DH: supervision and writing-review and editing. GG: writing-review and editing. DY: investigation and formal analysis. BP: data and formal analysis. JF: drafting the work and revising manuscript critically.

FUNDING

This work was supported by the National Nonprofit Fundamental Research Grant of China, Institute of Geology, China, Earthquake Administration (IGCEA), and this research was supported by the National Natural Science Foundation of China (41872254 and 41911540472) and China Scholarship Council.

ACKNOWLEDGMENTS

The authors thank H.Q. Wei for the support during the field work and valuable suggestions. The authors also thank the two referees for the constructive reviews of the manuscript.

REFERENCES

Andreeva, O. A., Yarmolyuk, V. V., Andreeva, I. A., Ji, J. Q., and Li, W. R. (2014). The Composition and Sources of Magmas of Changbaishan Tianchi Volcano (China-North Korea). *Dokl. Earth Sc.* 456, 572–578. doi:10.1134/s1028334x14050213

Basu, A. R., Wang Junwen, J., Huang Wankang, W., Xie Guanghong, G., and Tatsumoto, M. (1991). Major Element, REE, and Pb, Nd and Sr Isotopic Geochemistry of Cenozoic Volcanic Rocks of Eastern China: Implications for Their Origin from Suboceanic-type Mantle Reservoirs. *Earth Planet. Sci. Lett.* 105, 149–169. doi:10.1016/0012-821x(91)90127-4

Bgmrjp (1988). *Regional Geological Records of Jilin Province*, 260–280. (in Chinese).Bureau of Geology and mineral Resources of Jilin Province

Bizzarro, M., Simonetti, A., Stevenson, R. K., and David, J. (2002). Hf Isotope Evidence for a Hidden Mantle Reservoir. *Geol* 30 (9), 771. doi:10.1130/0091-7613(2002)030<0771:hiefah>2.0.co;2

Borisova, A. Y., Bindeman, I. N., Toplis, M. J., Zagrtdenov, N. R., Guignard, J., Safonov, O. G., et al. (2020). Zircon Survival in Shallow Asthenosphere and Deep Lithosphere. *Am. Mineral.* 105, 1662–1671. doi:10.2138/am-2020-7402

Boynton, W. V. (1984). "Cosmochemistry of the Rare Earth Elements: Meteorite Studies," in *Rare Earth Element Geochemistry: Developments in Geochemistry*. Editor P. Henderson (Elsevier), 2, 63–114. doi:10.1016/b978-0-444-42148-7.50008-3

Chen, L.-H., Zeng, G., Jiang, S.-Y., Hofmann, A. W., Xu, X.-S., and Pan, M.-B. (2009). Sources of Anfengshan Basalts: Subducted Lower Crust in the Sulu UHP belt, China. *Earth Planet. Sci. Lett.* 286, 426–435. doi:10.1016/j.epsl.2009.07.006

Chen, Y., Ai, Y., Jiang, M., Yang, Y., and Lei, J. (2021). New Insights into Potassic Intraplate Volcanism in Northeast China from Joint Tomography of Ambient Noise and Teleseismic Surface Waves. *J. Geophys. Res. Solid Earth* 126, e2021JB021856. doi:10.1029/2021JB021856

Choi, H.-O., Choi, S. H., Lee, Y. S., Ryu, J.-S., Lee, D.-C., Lee, S.-G., et al. (2020). Petrogenesis and Mantle Source Characteristics of the Late Cenozoic Baekdusan (Changbaishan) Basalts, North China Craton. *Gondwana Res.* 78, 156–171. doi:10.1016/j.gr.2019.08.004

Condamine, P., and Médard, E. (2014). Experimental Melting of Phlogopite-Bearing Mantle at 1 GPa: Implications for Potassic Magmatism. *Earth Planet. Sci. Lett.* 397, 80–92. doi:10.1016/j.epsl.2014.04.027

Defant, M. J., and Drummond, M. S. (1990). Derivation of Some Modern Arc Magmas by Melting of Young Subducted Lithosphere. *Nature* 347, 662–665. doi:10.1038/347662a0

Deng, J. F. (2004). *Petrogenesis, Tectonic Setting and Mineralization*. Beijing: Geological Press, 3–129. (in Chinese).

Deng, J., Wang, Q., and Li, G. (2017). Tectonic Evolution, Superimposed Orogeny, and Composite Metallogenic System in China. *Gondwana Res.* 50, 216–266. doi:10.1016/j.gr.2017.02.005

Dobosi, G., Kempton, P. D., Downes, H., Embey-Isztin, A., Thirlwall, M., and Greenwood, P. (2003). Lower Crustal Granulite Xenoliths from the Pannonian Basin, Hungary, Part 2: Sr-Nd-Pb-Hf and O Isotope Evidence for Formation of continental Lower Crust by Tectonic Emplacement of Oceanic Crust. *Contrib. Mineral. Petrol.* 144, 671–683. doi:10.1007/s00410-002-0422-1

Fan, Q. C., Liu, R. X., Wei, H. Q., Sui, J. L., and Li, Ni. (1999). The Petrology and Geochemistry of Jinlongdingzi Modern Active Volcano in Longgang Area. *Acta Petrologica Sinica* 15, 584–589. (in Chinese with English abstract).

Fan, X., Chen, Q.-F., Ai, Y., Chen, L., Jiang, M., Wu, Q., et al. (2021). Quaternary Sodic and Potassic Intraplate Volcanism in Northeast China Controlled by the Underlying Heterogeneous Lithospheric Structures. *Geology* 49. doi:10.1130/G48932.1

Foley, S., and Peccerillo, A. (1992). Potassic and Ultrapotassic Magmas and Their Origin. *Lithos* 28, 181–185. doi:10.1016/0024-4937(92)90005-j

Furman, T., and Graham, D. (1999). Erosion of Lithospheric Mantle beneath the East African Rift System: Geochemical Evidence from the Kivu Volcanic Province. *Lithos* 48, 237–262. doi:10.1016/s0024-4937(99)00031-6

Ge, W. C., Liu, R. X., Li, Z. X., and Zhou, H. W. (2001). Mafic Intrusions in Longsheng Area: Age and its Geological Implications. *Chin. J. Geology.* 36, 112–118. (in Chinese with English abstract). doi:10.3321/j.issn:0563-5020.2001.01.013

Ge, W., Zhao, G., Sun, D., Wu, F., and Lin, Q. (2003). Metamorphic P-T Path of the Southern Jilin Complex: Implications for Tectonic Evolution of the Eastern Block of the North China Craton. *Int. Geology. Rev.* 45, 1029–1043. doi:10.2747/0020-6814.45.11.1029

Gilder, S. A., Gill, J., Coe, R. S., Zhao, X., Liu, Z., Wang, G., et al. (1996). Isotopic and Paleomagnetic Constraints on the Mesozoic Tectonic Evolution of South China. *J. Geophys. Res.* 101, 16137–16154. doi:10.1029/96jb00662

Gilder, S. A., Keller, G. R., Luo, M., and Goodell, P. C. (1991). Eastern Asia and the Western Pacific Timing and Spatial Distribution of Rifting in China. *Tectonophysics* 197, 225–243. doi:10.1016/0040-1951(91)90043-r

Hoskin, P. W. O., and Schaltegger, U. (2003). 2. The Composition of Zircon and Igneous and Metamorphic Petrogenesis. *Rev. Mineralogy Geochem.* 53, 27–62. doi:10.1515/9781501509322-005

Jin, B. L., and Zhang, X. Y. (1994). *Researching Volcanic Geology in Mount Changbai*. Yanji: Northeast Korean Nationality Education Press, 1–223. (in Chinese).

Kuritani, T., Kimura, J.-I., Miyamoto, T., Wei, H., Shimano, T., Maeno, F., et al. (2009). Intraplate Magmatism Related to Deceleration of Upwelling Asthenospheric Mantle: Implications from the Changbaishan Shield Basalts, Northeast China. *Lithos* 112, 247–258. doi:10.1016/j.lithos.2009.02.007

Lee, S. H., Oh, C. W., Lee, Y. S., Lee, S.-G., and Liu, J.-q. (2021). Petrogenesis of the Cenozoic Volcanic Rocks in Baekdu Volcano in Northeastern Asia and the Expected Depth of the Magma Chamber Based on Geochemistry, mineral Chemistry, and Sr-Nd-Pb Isotope Chemistry. *Lithos* 388-389, 106080. doi:10.1016/j.lithos.2021.106080

Lei, M., Guo, Z., Zhao, W., Zhang, M., and Ma, L. (2020). Coexisting Late Cenozoic Potassic and Sodic Basalts in NE China: Role of Recycled Oceanic Components in Intraplate Magmatism and Mantle Heterogeneity. *Lithosphere* 2020, 8875012. doi:10.2113/2020/8875012

Li, C. N. (1992). *Trace Element Petrology of Igneous Rocks*. Wuhan: China University of Geosciences Press, 94–120. (in Chinese).

Li, C., and van der Hilst, R. D. (2010). Structure of the Upper Mantle and Transition Zone beneath Southeast Asia from Traveltime Tomography. *J. Geophys. Res.* 115, B07308. doi:10.1029/2009jb006882

Liu, J.-q., Chen, S.-s., Guo, Z.-f., Guo, W.-f., He, H.-y., You, H.-t., et al. (2015). Geological Background and Geodynamic Mechanism of MT. Changbai Volcanoes on the China-Korea Border. *Lithos* 236-237, 46–73. doi:10.1016/j.lithos.2015.08.011

Liu, J., Chu, G., Han, J., Rioual, P., Jiao, W., and Wang, K. (2009). Volcanic Eruptions in the Longgang Volcanic Field, Northeastern China, during the Past 15,000 Years. *J. Asian Earth Sci.* 34, 645–654. doi:10.1016/j.jseaes.2008.09.005

Liu, J. Q. (1981). *Cenozoic Volcanic Activity in Changbaishan Area, Master Thisis*. Beijing, China: Institute of Geology, Chinese Academy of Sciences, 1–38. (in Chinese with English abstract).

Liu, R. X., Xie, G. H., and Ni, J. Z. (1982). Petrographic Characteristics and Several Other Related Problems of the Layered Basic-Ultrabasic Intrusives in the Upper Yangtze Valley. *Geochemistry* 1, 51–68.

Liu, Y., Gao, S., Kelemen, P. B., and Xu, W. (2008). Recycled Crust Controls Contrasting Source Compositions of Mesozoic and Cenozoic Basalts in the North China Craton. *Geochimica et Cosmochimica Acta* 72, 2349–2376. doi:10.1016/j.gca.2008.02.018

Lynner, C., and Long, M. D. (2014). Sub-slab Anisotropy beneath the Sumatra and Circum-Pacific Subduction Zones from Source-Side Shear Wave Splitting Observations. *Geochem. Geophys. Geosyst.* 15, 2262–2281. doi:10.1002/2014gc005239

Ma, H. R., Yang, Q. F., Pan, X. D., Wu, C. Z., and Chen, C. (2015). Origin of Early Pleistocene Basaltic Lavas in the Erdaobaihe River basin, Changbaishan Region. *Acta Petrologica Sinica* 31, 3484–3494. (in Chinese with English abstract). doi:10.1007/s10114-015-3140-0

Ma, J., Tian, Y., Zhao, D., Liu, C., and Liu, T. (2019). Mantle Dynamics of Western Pacific and East Asia: New Insights from P Wave Anisotropic Tomography. *Geochem. Geophys. Geosyst.* 20, 3628–3658. doi:10.1029/2019gc008373

Mao, J. W., Cheng, Y. B., Chen, M. B., and Franco, P. (2013). Major Types and Time–Space Distribution of Mesozoic Ore Deposits in South China and Their Geodynamic Settings. *Mineralium Deposita* 48, 267–294. doi:10.1007/s00126-012-0446-z

Mao, J. W., and Wang, Z. L. (2000). A Preliminary Study on Time Limits and Geodynamic Setting of Large-Scale Matellogeny in East China. *Minaral Deposits* 19, 403–405. (in Chinese with English abstract). doi:10.3969/j.issn.0258-7106.2000.04.001

Ouyang, H., Wu, X., Mao, J., Su, H., Santosh, M., Zhou, Z., et al. (2014). The Nature and Timing of Ore Formation in the Budunhua Copper deposit, Southern Great Xing'an Range: Evidence from Geology, Fluid Inclusions, and U-Pb and Re-os Geochronology. *Ore Geology. Rev.* 63, 238–251. doi:10.1016/j.oregeorev.2014.05.016

Pan, B., de Silva, S. L., Xu, J., Liu, S., and Xu, D. (2020). Late Pleistocene to Present Day Eruptive History of the Changbaishan-Tianchi Volcano, China/DPRK: New Field, Geochronological and Chemical Constraints. *J. Volcanology Geothermal Res.* 399, 106870. doi:10.1016/j.jvolgeores.2020.106870

Puffer, J. H. (2001). Contrasting High Field Strength Element Contents of continental Flood Basalts from Plume versus Reactivated-Arc Sources. *Geol* 29, 675–678. doi:10.1130/0091-7613(2001)029<0675:chfsec>2.0.co;2

Sisson, T. W., Ratajeski, K., Hankins, W. B., and Glazner, A. F. (2005). Voluminous Granitic Magmas from Common Basaltic Sources. *Contrib. Mineral. Petrol.* 148, 635–661. doi:10.1007/s00410-004-0632-9

Sun, J.-G., Han, S.-J., Zhang, Y., Xing, S.-W., and Bai, L.-A. (2013). Diagenesis and Metallogenetic Mechanisms of the Tuanjiegou Gold deposit from the Lesser Xing'an Range, NE China: Zircon U-Pb Geochronology and Lu-Hf Isotopic Constraints. *J. Asian Earth Sci.* 62, 373–388. doi:10.1016/j.jseaes.2012.10.021

Sun, J. G., Zhang, Y., Xing, S. W., Zhao, K. Q., Zhang, Z. J., Bai, L. A., et al. (2012). Genetic Types, Ore-Forming Age and Geodynamic Setting of Endogenic

Molybdenum Deposits in the Eastern Edge of Xing-Meng Orogenic belt. *Acta Petrologica Sinica* 28, 1317–1332. (in Chinese with English abstract).

Sun, S.-s., and McDonough, W. F. (1989). Chemical and Isotopic Systematics of Oceanic Basalts: Implications for Mantle Composition and Processes. *Geol. Soc. Lond. Spec. Publications* 42, 313–345. doi:10.1144/gsl.sp.1989.042.01.19

Sun, Y., Teng, F.-Z., Pang, K.-N., Ying, J.-F., and Kuehner, S. (2021). Multistage Mantle Metasomatism Deciphered by Mg–Sr–Nd–Pb Isotopes in the Leucite Hills Lamproites. *Contrib. Mineral. Petrol.* 176, 45. doi:10.1007/s00410-021-01801-9

Sun, Y., Ying, J., Zhou, X., Shao, J. a., Chu, Z., and Su, B. (2014). Geochemistry of Ultrapotassic Volcanic Rocks in Xiaogulihe NE China: Implications for the Role of Ancient Subducted Sediments. *Lithos* 208-209, 53–66. doi:10.1016/j.lithos.2014.08.026

Takeshi, K., Mitsuhiro, N., Jumpei, N., Tetsuya, Y., and Tsuyoshi, M. (2020). Magma Plumbing System for the Millennium Eruption at Changbaishan Volcano, China: Constraints from Whole-Rock U–Th Disequilibrium. *Lithos* 366-367, 105564. doi:10.1016/j.lithos.2020.105564

Tang, Y., Obayashi, M., Niu, F., Grand, S. P., Chen, Y. J., Kawakatsu, H., et al. (2014). Changbaishan Volcanism in Northeast China Linked to Subduction-Induced Mantle Upwelling. *Nat. Geosci* 7, 470–475. doi:10.1038/ngeo2166

Tian, Y., Zhu, H., Zhao, D., Liu, C., Feng, X., Liu, T., et al. (2016). Mantle Transition Zone Structure beneath the Changbai Volcano: Insight into Deep Slab Dehydration and Hot Upwelling Near the 410 Km Discontinuity. *J. Geophys. Res. Solid Earth* 121, 5794–5808. doi:10.1002/2016JB0129510.1002/2016jb012959

Wang, F., Chen, W. J., Peng, Z. C., and Li, Q. (2001). Activity of Changbaishan Tianchi Volcano since Late Pleistocene:The Constrain from Geochronology of High Precision U-Series TIMS Method. *Geochimica* 30, 88–94.

Wang, F., Chen, W. J., Peng, Z. C., Zhang, Z. L., and Hu, Y. T. (1999). Chronology of Young Volcanic Rocks of Changbaishan Tianchi and Tengchong, China, by Using the Uranium-Series TIMS Method. *Geol. Rev.* 45, 914–925. (in Chinese with English abstract). doi:10.16509/j.georeview.1999.s1.003

Wang, X.-C., Wilde, S. A., Li, Q.-L., and Yang, Y.-N. (2015). Continental Flood Basalts Derived from the Hydrous Mantle Transition Zone. *Nat. Commun.* 6, 7700. doi:10.1038/ncomms8700

Wang, X., Chen, Q. F., Niu, F., Wei, S., and Liu, L. (2020). Distinct Slab Interfaces Imaged within the Mantle Transition Zone. *Nat. Geosci.* 13, 1–6. doi:10.1038/s41561-020-00653-5

Wang, Y., Li, C., Wei, H., and Shan, X. (2003). Late Pliocene-Recent Tectonic Setting for the Tianchi Volcanic Zone, Changbai Mountains, Northeast China. *J. Asian Earth Sci.* 21, 1159–1170. doi:10.1016/s1367-9120(03)00019-1

Wang, Y., Zhao, Z.-F., Zheng, Y.-F., and Zhang, J.-J. (2011). Geochemical Constraints on the Nature of Mantle Source for Cenozoic Continental Basalts in East-Central China. *Lithos* 125, 940–955. doi:10.1016/j.lithos.2011.05.007

Wei, H., Wang, Y., Jin, J., Gao, L., Yun, S.-H., and Jin, B. (2007). Timescale and Evolution of the Intracontinental Tianchi Volcanic Shield and Ignimbrite-Forming Eruption, Changbaishan, Northeast China. *Lithos* 96, 315–324. doi:10.1016/j.lithos.2006.10.004

Wiedenbeck, M., Allé, P., Corfu, F., Griffin, W. L., Meier, M., Oberli, A., et al. (1995). Three Natural Zircon Standards for U-Th-Pb, Lu-Hf, Trace Element and REE Analyses. *Geostandards Newsl.* 19, 1–23. doi:10.1111/j.1751-908x.1995.tb00147.x

Wu, F.-Y., Sun, D.-Y., Ge, W.-C., Zhang, Y.-B., Grant, M. L., Wilde, S. A., et al. (2011). Geochronology of the Phanerozoic Granitoids in Northeastern china. *J. Asian Earth Sci.* 41, 1–30. doi:10.1016/j.jseaes.2010.11.014

Wu, F.-y., Sun, D.-y., Li, H., Jahn, B.-m., and Wilde, S. (2002). A-type Granites in Northeastern China: Age and Geochemical Constraints on Their Petrogenesis. *Chem. Geology.* 187, 143–173. doi:10.1016/s0009-2541(02)00018-9

Wu, F. Y., Li, X. H., Zheng, Y. F., and Gao, S. (2007). Lu-Hf Isotopic Systematics and Their Applications in Petrology. *Acta Petrologica Sinica* 23, 185–220. (in Chinese with English abstract). doi:10.1007/s10255-007-0392-1

Wu, F., Zhao, G., Wilde, S. A., and Sun, D. (2005). Nd Isotopic Constraints on Crustal Formation in the North China Craton. *J. Asian Earth Sci.* 24, 523–545. doi:10.1016/j.jseaes.2003.10.011

Wyllie, P. J., and Sekine, T. (1982). The Formation of Mantle Phlogopite in Subduction Zone Hybridization. *Contr. Mineral. Petrol.* 79, 375–380. doi:10.1007/bf01132067

Xu, J. D., Yu, H. M., and Zhao, B. (2013a). Petrographic and Micro-textural Features of the Yellow Pumice at Tianwen Peak of Changbaishan Tianchi Volcano. *Seismology Geology.* 35, 363–370. (in Chinese with English abstract). doi:10.3969/j.issn.0253-4967.2013.02.014

Xu, S., Zheng, G., Nakai, S. i., Wakita, H., Wang, X., and Guo, Z. (2013b). Hydrothermal He and CO2 at Wudalianchi Intra-plate Volcano, NE China. *J. Asian Earth Sci.* 62, 526–530. doi:10.1016/j.jseaes.2012.11.001

Xu, W. L., Chen, J. H., Weng, A. H., Tang, J., Wang, F., Wang, C. G., et al. (2020a). Stagnant Slab Front within the Mantle Transition Zone Controls the Formation of Cenozoic Intracontinental High-Mg Andesites in Northeast Asia. *Geology* 48, 1–6. doi:10.1130/g47917.1

Xu, Y.-G., Ma, J.-L., Frey, F. A., Feigenson, M. D., and Liu, J.-F. (2005). Role of Lithosphere-Asthenosphere Interaction in the Genesis of Quaternary Alkali and Tholeiitic Basalts from Datong, Western North China Craton. *Chem. Geology.* 224, 247–271. doi:10.1016/j.chemgeo.2005.08.004

Xu, Y.-G., Zhang, H.-H., Qiu, H.-N., Ge, W.-C., and Wu, F.-Y. (2012). Oceanic Crust Components in continental Basalts from Shuangliao, Northeast China: Derived from the Mantle Transition Zone? *Chem. Geology.* 328, 168–184. doi:10.1016/j.chemgeo.2012.01.027

Xu, Z.-t., Liu, Y., Sun, J.-g., Liang, X.-l., and Xu, Z.-k. (2020b). Nature and Ore Formation of the Erdaohezi Pb-Zn deposit in the Great Xing'an Range, NE China. *Ore Geology. Rev.* 119, 103385. doi:10.1016/j.oregeorev.2020.103385

Zartman, R. E., and Doe, B. R. (1981). Plumbotectonics-the Model. *Tectonophysics* 75, 135–162. doi:10.1016/0040-1951(81)90213-4

Zhai, M. G., Zhu, X. Y., Zhou, Y. Y., Zhao, L., and Zhou, L. (2019). Continental Crustal Evolution and Synchronous Metallogeny Through Time in the North Chian Craton. *J. Asian Earth Sci.* 194, 104169. doi:10.1016/j.jseaes.2019.104169

Zhang, J.-J., Zheng, Y.-F., and Zhao, Z.-F. (2009). Geochemical Evidence for Interaction between Oceanic Crust and Lithospheric Mantle in the Origin of Cenozoic continental Basalts in East-central China. *Lithos* 110, 305–326. doi:10.1016/j.lithos.2009.01.006

Zhang, M., Guo, Z., Cheng, Z., Zhang, L., and Liu, J. (2015). Late Cenozoic Intraplate Volcanism in Changbai Volcanic Field, on the Border of china and north korea: Insights into Deep Subduction of the pacific Slab and Intraplate Volcanism. *J. Geol. Soc.* 172, 648–663. doi:10.1144/jgs2014-080

Zhang, M., Guo, Z., Liu, J., Liu, G., Zhang, L., Lei, M., et al. (2018). The Intraplate Changbaishan Volcanic Field (China/North Korea): A Review on Eruptive History, Magma Genesis, Geodynamic Significance, Recent Dynamics and Potential Hazards. *Earth-Science Rev.* 187, 19–52. doi:10.1016/j.earscirev.2018.07.011

Zhang, Y., Sun, J. G., Xing, S. W., Zhao, K. Q., Wang, Y., Qiu, D. M., et al. (2014). Diagenetic and Metallogenic Geochronology and Geochemical Characteristics of the Sifangdianzi Molybdenum Deposit in Jilin Province. *J. Jilin Univ. Earth Sci. Edition* 44, 1869–1882. (in Chinese with English abstract). doi:10.13278/j.cnki.jjuese.201406113

Zhang, Z. C., and Luo, W. J. (2011). Advances in Petrology, Geochemistry and Chronology of Cenozoic Volcanic Rocks in China. *Bull. Minerals, Petrol. Geochem.* 30, 353–360. (in Chinese). doi:10.3969/j.issn.1007-2802.2011.04.001

Zhao, Z. H. (2016). *Mechanisms of Trace Element Geochemistry*. the second edition. Beijing: Science Press, 3–443. (in Chinese).

Zheng, Y. F., Zhao, Z. F., Wu, Y. B., Zhang, S. B., Liu, X., and Wu, F. Y. (2006). Zircon U-Pb Age, Hf and O Isotope Constraints on Protolith Origin of Ultrahigh-Pressure Eclogite and Gneiss in the Dabie Orogen. *Chem. Geology.* 231 (1-2), 135–158. doi:10.1016/j.chemgeo.2006.01.005

Zheng, Y., Xu, Z., Zhao, Z., and Dai, L. (2018). Mesozoic Mafic Magmatism in North China: Implications for Thinning and Destruction of Cratonic Lithosphere. *Sci. China Earth Sci.* 61, 353–385. (in Chinese). doi:10.1007/s11430-017-9160-3

Zhi, X., Song, Y., Frey, F. A., Feng, J., and Zhai, M. (1990). Geochemistry of Hannuoba Basalts, Eastern China: Constraints on the Origin of Continental Alkalic and Tholeiitic Basalt. *Chem. Geology.* 88, 1–33. doi:10.1016/0009-2541(90)90101-c

Zhou, X., and Armstrong, R. (1982). Cenozoic Volcanic Rocks of Eastern China - Secular and Geographic Trends in Chemistry and Strontium Isotopic Composition. *Earth Planet. Sci. Lett.* 58, 301–329. doi:10.1016/0012-821x(82)90083-8

Zhou, X. M., and Li, W. X. (2000). Origin of Late Mesozoic Igneous Rocks in Southeastern China: Implications for Lithosphere Subduction and

Underplating of Mafic Magmas. *Tectonophysics* 326, 269–287. doi:10.1016/s0040-1951(00)00120-7

Zhu, B. (2007). Pb-Sr-Nd Isotopic Systematics of Mantle-Derived Rocks in the World. *Earth Sci. Front.* 14, 24–36. (in Chinese with English abstract). doi:10.1016/s1872-5791(07)60012-8

Zhu, H., Tian, Y., Zhao, D., Li, H., and Liu, C. (2019). Seismic Structure of the Changbai Intraplate Volcano in NE China from Joint Inversion of Ambient Noise and Receiver Functions. *J. Geophys. Res. Solid Earth* 124, 4984–5002. doi:10.1029/2018jb016600

Zhu, R. X., Chen, L., Wu, F. Y., and Liu, J. L. (2011). Time, Range and Mechanism of Destruction of the North China Craton, Science China. *Earth Sci.* 41, 583–592. (in Chinese). doi:10.1007/s11430-011-4203-4

Zindler, A., and Hart, S. (1986). Chemical Geodynamics. *Annu. Rev. Earth Planet. Sci.* 14, 493–571. doi:10.1146/annurev.ea.14.050186.002425

Zou, H. B., Fan, Q. C., and Yao, Y. C. (2008). U–Th Systematics of Dispersed Young Volcanoes in NE China: Asthenosphere Upwelling Caused by Piling up and Upward Thickening of Stagnant pacific Slab. *Chem. Geology.* 255 (1-2), 134–142. doi:10.1016/j.chemgeo.2008.06.022

Zou, H., Fan, Q., and Zhang, H. (2010). Rapid Development of the Great Millennium Eruption of Changbaishan (Tianchi) Volcano, China/North Korea: Evidence from U-Th Zircon Dating. *Lithos* 119, 289–296. doi:10.1016/j.lithos.2010.07.006

Conflict of Interest: The authors declare that the research was conducted in the absence of any commercial or financial relationships that could be construed as a potential conflict of interest.

Publisher's Note: All claims expressed in this article are solely those of the authors and do not necessarily represent those of their affiliated organizations, or those of the publisher, the editors, and the reviewers. Any product that may be evaluated in this article, or claim that may be made by its manufacturer, is not guaranteed or endorsed by the publisher.